Arboreal topological and fracton phases

Nandagopal Manoj* and Vijay B. Shenoy†
Centre for Condensed Matter Theory, Department of Physics, Indian Institute of Science, Bangalore 560012, India

(Received 2 October 2022; accepted 10 April 2023; published 20 April 2023)

We describe topologically ordered and fracton-ordered quantum systems on geometries which do not have an underlying manifold structure. Using tree graphs such as the k-coordinated Bethe lattice $\mathrm{B}(k)$ and a hypertree called the (k, n)-hyper-Bethe lattice $\mathrm{HB}(k, n)$ consisting of k-coordinated hyperlinks (links defined by n sites), we construct multidimensional arboreal arenas such as $\mathrm{B}(k_1)\square\mathrm{B}(k_2)$ using a generalized notion of a graph Cartesian product $\square$. We study various quantum systems such as the $\mathbb{Z}_2$ gauge theory, generalized quantum Ising models (GQIMs), the fractonic X-cube model, and related X-cube gauge theory defined on these arboreal arenas, finding several fascinating results. Even the simplest $\mathbb{Z}_2$ gauge theory on a two-dimensional arboreal arena is found to be fractonic—an isolated monopole excitation is rendered fully immobile on an arboreal arena. The X-cube model on a generic three-dimensional arboreal arena is found to be fully fractonic in the magnetic sector, i.e., all multipoles of magnetic excitations are rendered immobile on the arboreal arena. We obtain variational ground state phase diagrams of the gauge theories (both $\mathbb{Z}_2$ and X-cube gauge theories) which are shown to have deconfined and confined phases. These phases are usually separated by a first-order transition, while continuous transitions are obtained in some cases. Further, we find an intriguing class of dualities in arboreal arenas, as illustrated by the $\mathbb{Z}_2$ gauge theory defined on $\mathrm{B}(k_1)\square\mathrm{B}(k_2)$ being dual to a GQIM defined on $HB(2, k_1)\square HB(2, k_2)$. Finally, we discuss different classes of topological and fracton orders that appear on arboreal arenas. We find three distinct classes of arboreal toric code orders on two-dimensional arboreal arenas, those that occur on $\mathrm{B}(2)\square\mathrm{B}(2)$, $\mathrm{B}(k)\square\mathrm{B}(2)$, $k > 2$, and $\mathrm{B}(k_1)\square\mathrm{B}(k_2)$, $k_1, k_2 > 2$. Likewise, four classes of X-cube fracton orders are found on three-dimensional arboreal arenas which correspond to those on $\mathrm{B}(2)\square\mathrm{B}(2)\square\mathrm{B}(2)$, $\mathrm{B}(k)\square\mathrm{B}(2)\square\mathrm{B}(2)$, $k > 2$, $\mathrm{B}(k_1)\square\mathrm{B}(k_2)\square\mathrm{B}(2)$, $k_1, k_2 > 2$, and $\mathrm{B}(k_1)\square\mathrm{B}(k_2)\square\mathrm{B}(k_3)$, $k_1, k_2, k_3 > 2$.

DOI: 10.1103/PhysRevB.107.165136

I. INTRODUCTION

A central problem of condensed matter physics is the description and classification of phases of systems with many microscopic quantum degrees of freedom. Research over the last two decades has revealed that, in addition to the ideas of symmetry, notions of entanglement and topology have a preeminent role in the description and classification of phases [1–5]. Broadly, quantum phases realized by many degrees of freedom can be classified as short-ranged entangled or long-range entangled with topological order and complex patterns of entanglement. Examples of unique phases already realized in the laboratory with short-range entanglement are topological insulators [4,6,7]. Similarly, fractional hall states [8] realize states with topological order and associated long-range entanglement.

Topologically ordered phases have enjoyed particular attention owing to their exotic properties that can be exploited for topologically protected quantum information processing [9]. A particularly interesting example of a topologically ordered system useful as a quantum memory is the toric code [10]. The toric code has a ground state degeneracy that depends only on the topology of the manifold on which it is defined, and not on the microscopic details such as lattice structure. For example, the ground state degeneracy of a toric code defined on a torus is 4 irrespective of whether the underlying lattice is a square lattice or a triangular lattice. Excitations of the toric code also have exotic physics—the two types of excitations, magnetic monopoles (plaquette excitations), and electric charges (vertex excitations) are mutually semionic, and bound states of these excitations are fermions (see Ref. [11] that explores interesting consequences and implications of this). From the perspective of quantum information processing/computing, the ground state degeneracy which is topologically protected is an attractive platform to store and manipulate quantum information [12–14]. A deeper understanding of topologically ordered phases was effected with the formulations of many exactly solvable models, for example, string-net models [5,15]. Connections to topological field theories and modular tensor categories have been exploited for the classification (see recent work [16] and references therein) of topologically ordered phases.

Although topologically ordered phases have degenerate ground states that are protected, there are issues associated with the stability of these phases at finite temperatures [13,14,17–19]. This arises from the fact that the monopole excitations discussed above, when thermally excited in pairs, can proliferate, owing to the entropy gain. This, and related issues, have prompted researchers to formulate and explore models

*Present address: Department of Physics, California Institute of Technology, Pasadena, CA 91125, USA; nmanoj@caltech.edu
†shenoy@iisc.ac.in

[20–22,22–29] where the excitations have limited mobility, possibly offering avenues to address the finite-temperature issues faced by topological codes, giving way to the discovery of fracton phases (see reviews [30,31]). Fracton phases are so named owing to the fact that the excitations in this systems have fractional mobility. As an example, the excitations of the exactly solvable X-cube model, the toric-code of fracton physics, has point magnetic monopoles which are fully immobile, even as the dipoles of these magnetic monopoles are mobile in a plane. The analogs of electric charges can be moved along a line by local operations. While the presence of immobile excitations is a generic feature of all fracton phases, some, like the X-cube model discussed above, have bound states of excitations that are mobile. On the other hand, models such as Haah's code [23] have only immobile excitations, leading to further classification of fracton phases as type-I and type-II fractons (see Ref. [31]). Another intriguing aspect of fracton phases is that they have a subextensive ground state degeneracy, i.e., the degeneracy scales as, for example, in the X-cube model, e^{aL}, where L is the length of the side of the cuboidal box with periodic boundary conditions used to define the model and a is a numerical constant. In addition, this ground state degeneracy, although subextensive, depends on the details of the lattice, leading them to be termed geometrically ordered [32]. Based on these cues, the notion of foliated fracton order has been formulated and elaborated [33,34]. Yet another notable point is that discrete fracton models (such as the X-cube model) which are typically theories with a local gauge structure have been shown [27] to be dual to discrete models with global subsystem symmetries where the symmetry operations act on a subextensive set of degrees of freedom.

The discrete models discussed above have motivated long-wavelength descriptions (field-theoretic descriptions) of topologically ordered and fracton phases. As alluded to above, topological field theories are used to describe topologically ordered phases. For example, Chern-Simons theories with a suitably chosen K matrix, a topological field theory, can describe topologically ordered phases of the toric code [10] and the double-semion model [15]. In such theories, the gauge fields are assigned to every space-time point of the manifold of interest, and the action depends on these gauge fields only via a topological invariant associated with these fields. The field theoretical description of fracton phases have more interesting underpinnings. Anticipated by work aimed at providing infrared descriptions of quantum spin liquids [35,36], Refs. [37,38] elaborated that higher rank tensor gauge theories offer themselves as natural candidates for the long-wavelength descriptions of fracton phases. Generalizations to include extended charges with different types of mobility restrictions have also been explored [39,40], and general fracton gauge principles have been formulated and studied [41,42]. Remarkably, some of these higher rank tensor gauge theories have been shown to be dual [43–46] to many well-known and well-studied [47–50] systems. Field theories related to the discrete fracton models discussed above have also been postulated [51–54].

As is clear from the discussion above, key advances have been made possible by the formulation of discrete models. These discrete models are typically defined on lattices that tessellate a manifold. For example, the square lattice with periodic boundary conditions tessellates the two-torus. The Chern-Simons theory [8] that describes the toric code uses topological data associated with $U(1)$ gauge fields that are attached at points of the two-torus (and, of course, the time coordinate), i.e., the manifold that the discrete square lattice tessellates. Our point here is that most of the discrete models defined and studied are on lattices that tessellate a manifold, and such models often enjoy the advantage of a universal long-wavelength field theoretical description using fields attached to points on that manifold. In other words, much of the current focus has been on systems defined on a manifold arena.

The creation, manipulation, and study of many-body quantum systems have seen spectacular advances in the last decade (see, for example, Ref. [55] and references in that issue). A number of platforms offer many opportunities to engineer a variety of discrete models, for example, circuit quantum electrodynamics [56] can be used to create topological codes and its excitations (see, for example, Refs. [57–59]). In this context, the unprecedented ability to control individual quantum degrees of freedom raises the possibility of exploring discrete quantum systems that are built on *nonmanifold arenas*. In other words, systems whose degrees of freedom are placed in a fashion different from the tessellation of a manifold. The main thrust of this paper is to explore this direction, i.e., to study many-body quantum systems that are defined on an arena that is not a discretization of a manifold.

At first glance, the problem statement seems unwieldy as there is a myriad of nonmanifold structures on which quantum models can be defined. Here we focus on those discrete arenas that are templated on tree graphs [60], which we dub the *arboreal arena*. Further, we focus on arenas that allow us to keep a notion of translational invariance and this restriction gives us a well-defined class of tree graphs that provide us the templates for the construction of the arboreal arena studied here. The key tree graph that we consider in our work is the k-Bethe lattice, denoted as $\mathrm{B}(k)$, which is an infinite graph where every vertex (or site) has k links/edges (each link, as usual, is defined by two graph vertices/sites) attached to it. A generalized tree graph, called a hypertree graph [60], also plays a crucial role in our discussion. A hypertree is a tree graph whose links, called hyperlinks, have an arbitrary number of sites attached to it. This leads naturally to a (k, n)-hyper-Bethe lattice denoted as $\mathrm{HB}(k, n)$, where each vertex(site) has k hyperlinks attached and each hyperlink has n vertices(sites) that define it. Next, we use a generalized notion of graph Cartesian product, denoted by $\square$, to construct higher dimensional arboreal arenas, for example, $\mathrm{B}(3)\square\mathrm{B}(2)$ is a two-dimensional arboreal arena. To explore the physics of models defined on these arboreal arenas, we also define finite arboreal arenas made from the ones defined above by the introduction of surfaces (of course, the sites/links on these surfaces will have a different environment than than the bulk, breaking the notion of translational symmetry in a controlled fashion).

Physics in arenas based on tree graphs have been studied in the past in various contexts, including classical statistical mechanics [61,62], physics of interacting fermions [63,64], etc. to state a few, where, oftentimes, exact solutions are possible in the limit of large coordination number (for example, $\mathrm{B}(k)$, for large k). Our motivation is to use tree graphs from

a different perspective—to create connectivities of underlying microscopic degrees of freedom (qubits) that produce different and varied patterns of quantum entanglement which could possibly offer unqiue opportunities, for example, in quantum information processing.

Following the definition of the arboreal arenas, we define and study a variety of models on them. In particular, we provide natural definitions of the $\mathbb{Z}_2$-gauge theory, generalized quantum Ising models (GQIMs) where interactions are defined on hyperlinks, the X-cube model and related X-cube gauge theory on arboreal arenas. We summarize here what we believe are intriguing and exciting results. First, we find that even the simple $\mathbb{Z}_2$ gauge theory on a two-dimensional arboreal arena is fractonic—isolated monopole excitations are fully immobile. Second, the X-cube model on a generic three-dimensional arboreal arena is fully fractonic in the magnetic sector; no multipole of magnetic excitation is mobile. Third, the gauge theories (both $\mathbb{Z}_2$ and X-cube gauge theories) have deconfined and confined phases at zero temperature that are generically separated by a first-order transition upon tuning of the electric coupling constant (second-order transitions are also possible). Fourth, we demonstrate a rich class of dualities between the models defined on an arboreal arena. An illustration: We show that the $\mathbb{Z}_2$ gauge theory defined on $\mathrm{B}(k_1)\square\mathrm{B}(k_2)$ is dual to a GQIM defined on $\mathrm{HB}(2,k_1)\square\mathrm{HB}(2,k_2)$ where the latter model possesses subsystem symmetries! These dualities are natural generalizations of the dualities formulated in Ref. [27] to the arboreal arena. Finally, we show a rather intriguing and aesthetically appealing result. We show that there are only three distinct classes of arboreal toric code orders on the two-dimensional arboreal arenas, those that correspond to $\mathrm{B}(2)\square\mathrm{B}(2)$, $\mathrm{B}(k)\square\mathrm{B}(2)$, $k>2$, and $\mathrm{B}(k_1)\square\mathrm{B}(k_2)$, $k_1,k_2>2$. This implies, for example, that the ground state of $\mathbb{Z}_2$ gauge theory defined on $\mathrm{B}(3)\square\mathrm{B}(3)$ in its deconfined phase, can be transformed to that of $\mathrm{B}(k_1)\square\mathrm{B}(k_2)$, for *any* $k_1>3$, $k_2>3$ by a finite depth unitary quantum circuit! Similarly, there are four classes of X-cube fracton orders on three-dimensional arboreal arenas viz., those that correspond to $\mathrm{B}(2)\square\mathrm{B}(2)\square\mathrm{B}(2)$, $\mathrm{B}(k)\square\mathrm{B}(2)\square\mathrm{B}(2)$, $k>2$, and $\mathrm{B}(k_1)\square\mathrm{B}(k_2)\square\mathrm{B}(2)$, $k_1,k_2>2$, and $\mathrm{B}(k_1)\square\mathrm{B}(k_2)\square\mathrm{B}(k_3)$, $k_1,k_2,k_3>2$.

In the next section, we present definitions of the various arboreal arena. This is followed by a discussion of arboreal $\mathbb{Z}_2$ gauge theory in Sec. III. The X-cube model and related gauge theory in the arboreal setting are discussed in Sec. IV. Arboreal topological and fracton orders and their classification are discussed in Sec V. Section VI concludes the paper with a discussion of arboreal quantum phases and possible applications, and directions of future research.

II. THE ARBOREAL ARENA

We adopt and adapt notions from graph theory to define arboreal arenas. A graph $\mathcal{G}=\{\mathcal{S},\mathcal{L}\}$ is a set of vertices $\mathcal{S}$ and a set of edges $\mathcal{L}$ that define connections between the vertices. In our discussion, we use the term sites synonymous with vertices and links also mean edges. Two sites are called adjacent if there is a link between them; we sometimes call adjacent sites neighbors. We consider only graphs whose links connect distinct sites, i.e., there are no links that start and end at the same site. However, links that connect to only a single site are allowed. A path on graph $\mathcal{G}$ is defined as an ordered (possibly repeating) list of sites such that adjacent elements in the ordered list are neighbors in $\mathcal{G}$. A loop is a path that starts and ends at the same site such that no other site is present more than once. A *tree*, denoted by T, is a graph that does not have any loops.

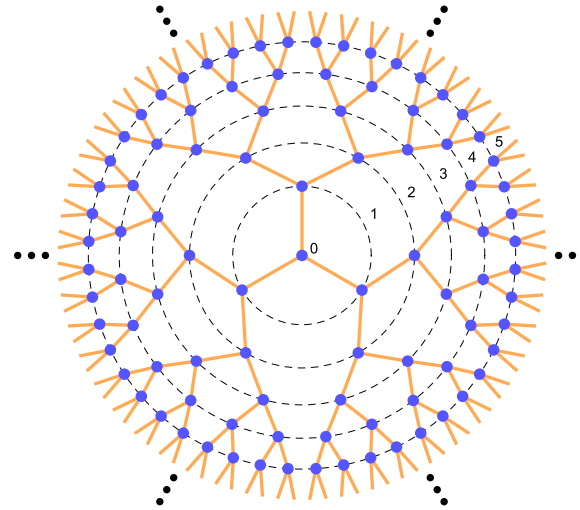

FIG. 1. Bethe lattice $\mathrm{B}(k)$ with $k=3$. The tree is infinite, as indicated by the radial black ellipses. The numbers indicate the generation g; all the sites on the same dashed circles belong to the same generation.

We focus on tree graphs that possess additional properties, in particular, a notion of translational symmetry (we avoid a formal definition of this). Roughly, this means that every site in the graph has an identical neighborhood. A natural example of such a tree is a Bethe lattice (referred to as a regular tree in the mathematics literature). We introduce the notion of a k-Bethe lattice denoted as $\mathrm{B}(k)$ where each site is attached to k links. Translational symmetry then necessitates that this graph is infinite (see Fig. 1). We can impose a coordinate system on $\mathrm{B}(k)$ by introducing the notion of generations. Pick any site and declare it to be the generation $g=0$. All sites linked to the site at generation $g=0$ are said to be in generation $g=1$, and similarly for any other generation g. For any generation $g>0$, there are $k(k-1)^{g-1}$ sites which can be suitably numbered using m (see Fig. 1) where $m=0,\ldots,k(k-1)^{g-1}-1$. The coordinate of any site in $\mathrm{B}(k)$ is then given by (g,m).

An important extension of the tree graph that plays a prominent role in our paper is the notion of a *hypertree*. Hypergraphs [60] are graphs where the links can contain any number of vertices. The desideratum of translation symmetry again requires that all the links contain the same number of vertices (say n). These ideas allow us to generalize $\mathrm{B}(k)$ to a hypertree $\mathrm{HB}(k,n)$, called a (k,n)-hyper Bethe lattice. A general way of stating the no-loop condition for hypertrees is that there exists no finite subset of links such that every vertex that touches a link of this subset touches an even number of distinct links of the subset. Figure 2 shows $\mathrm{HB}(2,3)$ and $\mathrm{HB}(3,3)$. Again, we can set up a coordinate system on this hyper-Bethe lattice using the notion of generations (see Fig. 2). Note that $\mathrm{HB}(k,2)$ is same as $\mathrm{B}(k)$.

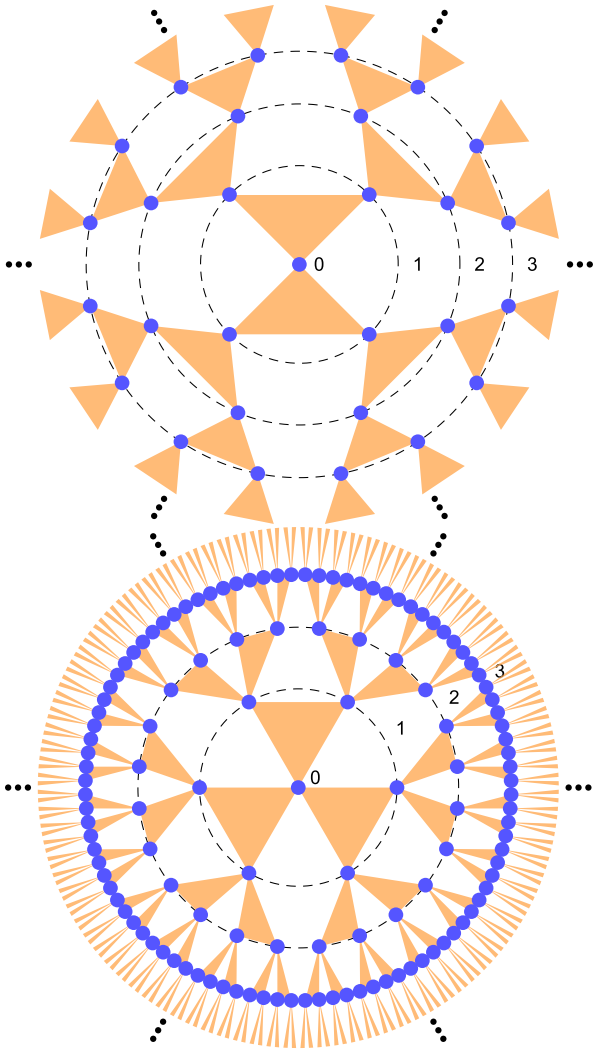

FIG. 2. Hyper-Bethe lattices HB(2, 3), and HB(3, 3). Hypertrees have generalized links (indicated by shaded triangles) which touch more than two sites (indicated by blue dots). As in Fig. 1, the numbers indicate the generation to which the sites belongs.

To understand the phases that appear on these arboreal arena, we also find it useful to break translational symmetry by introducing surfaces. A convenient way to achieve this goal is by truncating a HB(k, n) at some generation M (typically a large number), i.e., all sites up to and including generation M are kept. We call such hypertrees *hyper-Cayley trees*. A site of a hyper-Cayley tree is called an interior site if all the k links connected to it are present in the graph, and is termed a boundary site if the number of links connected to the site is less than k. Similarly, a hyperlink is called an interior link if there are n sites connected to it, and a boundary hyperlink otherwise. It is useful to define two types of hyper-Cayley trees. If the links connecting the sites of the Mth generation sites to the $M+1$-generation sites are kept in the graph, then these trees are termed *rough hyper-Cayley trees* and denoted by RHC$(k, n)_M$. In RHC$(k, n)_M$, all the sites are interior sites, while the last set of links (connecting Mth generation sites to $M+1$th generation sites) are boundary links (other links are interior links). If these boundary links are not included, then they are called *smooth hyper-Cayley trees* and denoted as SHC$(k, n)_M$. In SHC$(k, n)_M$, all links are interior links, while the sites of generation M are boundary sites (other sites are interior sites). For $n = 2$, RHC$(k, 2)_M$ and SHC$(k, 2)_M$ are denoted, respectively, as RC$(k)_M$ and SC$(k)_M$, i.e., rough and smooth Cayley trees.

Another important class of finite trees are useful for the discussion of arboreal quantum phases (especially in the construction of dual models). Choose a link in the infinite hyper-Bethe lattice HB(k, n) to be the central link, and declare its center as the origin. The n vertices touching this link are said to be at generation 1. The vertices adjacent to these links are of generation 2, and so on. This defines a unique coordinate system for the hyper-Bethe lattice. Now, as above, we can truncate the lattice at some generation M. For reasons that will become apparent in Sec. III F, we will call this lattice a *dual* smooth hyper-Cayley tree ($\widetilde{\text{SHC}}(k, n)_M$). We also define dual rough hyper-Cayley trees ($\widetilde{\text{RHC}}(k, n)_M$) as the lattice containing the sites up to generation M and keeping the boundary links that connect generation M to generation $M+1$ in this coordinate system. The (hyper)tree structures considered above, summarized in Table I, act as the building blocking for erecting arboreal arenas. Higher dimensional arboreal arenas can also be constructed in a natural fashion by using a generalization of a Cartesian product, called $\square$ for any two hypergraphs [60]. Let HT_1 and HT_2 be two hypertrees. Then, $\text{HT}_1 \square \text{HT}_2$ is also a hypergraph with sites that are the collection of ordered pairs of sites (u, v) where u is in HT_1 and v is in HT_2. A collection of l vertices $\{(u_1, v_1), (u_2, v_2), \ldots, (u_l, v_l)\}$ represent a hyperedge of $\text{HT}_1 \square \text{HT}_2$ if and only if, *one of the two conditions* are satisfied. Either, $u_1 = u_2 = \ldots = u_l$ and $(v_1, v_2, \ldots, v_l)$ is a hyperlink in HT_2, or $v_1 = v_2 = \ldots = v_l$ and $(u_1, u_2, \ldots, u_l)$ is a hyperlink in HT_1. Indeed, the $\square$-product HB$(k_1, n_1) \square$HB(k_2, n_2) will result in two-dimensional arboreal arenas with a hyperplaquette defined by $n_1 \times n_2$ sites with $n_1 + n_2$ hyperedges. The $\square$ product naturally generalizes to arbitrary dimensions d, for $\text{HT}_1 \square \text{HT}_2 \ldots \square \text{HT}_d$ is naturally defined recursively obtaining a *higher dimensional hypertree*. As an example, $\square^d$HB(k, n) has d-hypercubes with n^d sites and dn^{d-1}-hyperedges. We shall term HB$(k, 2) \square$HB$(2, 2) =$ B$(k) \square$B(2) as an *extruded* k tree.

It should be pointed out that the use of the term dimension here refers to the number of hypertrees used in the graph cartesian product $\square$ to construct the arboreal arena. Most importantly, the word dimension does *not* refer to the dimension of the underlying space in which these trees can be embedded. For example, B$(2) \square$B(2) can be embedded in a two-dimensional space, while B$(3) \square$B(2) cannot be embedded in a two-dimensional Cartesian space and requires a three-dimensional Cartesian space. In our terminology, *both* B$(2) \square$B(2) and B$(3) \square$B(2) are *two-dimensional* arboreal arenas.

A key point to be noted is that aside from whenever both k and n are not equal to 2 (we exclusively apply this condition when we refer to an arboreal arena), the HB(k, n) does not represent a tessellation of a manifold, in the sense a manifold is covered, for example, by simplices/cells [65].

TABLE I. Notation, nomenclature, and description of the tree graphs used to construct arboreal arenas.

Notation	Name	Description
$\mathrm{B}(k)$	k-Bethe lattice	Infinite translation invariant lattice with k links to each site (see Fig. 1)
$\mathrm{HB}(k,n)$	(k,n) hyper-Bethe lattice	Infinite translation invariant lattice with k generalized links to each site, and each generalized link containing n sites. (see Fig. 2)
$\mathrm{SHC}(k,n)_M$	$(k,n)_M$ hyper-Cayley tree (smooth boundaries)	Hyper-Cayley tree with M generations and k generalized links to each site except at boundary sites, which have only one link to it. All links contain n sites.
$\mathrm{RHC}(k,n)_M$	$(k,n)_M$ hyper-Cayley tree (rough boundaries)	Hyper-Cayley tree with M generations and k generalized links to every site. All links except the ones emanating out of the boundary sites (boundary links) contain n sites, and the boundary links contain only one site.
$\widetilde{\mathrm{SHC}}(k,n)_M$	$(k,n)_M$ dual hyper-Cayley tree (smooth boundaries)	Hyper-Cayley tree with an edge at the origin and M generations and k generalized links to each site except at boundary sites, which have only one link to it. All links contain n sites.
$\widetilde{\mathrm{RHC}}(k,n)_M$	$(k,n)_M$ dual hyper-Cayley tree (rough boundaries)	Hyper-Cayley tree with a generalized edge at the origin and M generations and k generalized links to every site. All (nonboundary) links contain n sites and the boundary links contain only one site.

These $\mathrm{HB}(k,n)$ with $k \neq 2$ or $n \neq 2$ offer a natural scaffold to construct nonmanifold arenas to explore possible new physics in them. Additionally, our construction has the advantage that $\square^d\mathrm{B}(2)$ indeed is the d-dimensional cubic lattice and so the physics of models defined on manifold arenas can be accessed in the same framework.

III. ARBOREAL GAUGE THEORIES

A. $\mathbb{Z}_2$ gauge theories

In this section, we will construct and study gauge theories on multidimensional arboreal arenas. We will focus on $\mathbb{Z}_2$ gauge structure. We begin with the two-dimensional arboreal arena: $\mathrm{B}(k_1)\square\mathrm{B}(k_2)$ with $k_1 > 2$. The coordinate of any site s on this arena is given by $((g_1, m_1), (g_2, m_2))$ where $g_i \in \{0, 1, 2, \ldots\}$, $m_i = 0, g_i = 0$ or $m_i \in \{0, 1, \ldots, k_i(k_i - 1)^{g_i - 1}\}$. The links are defined by unordered pairs of sites such as $[((g_1, m_1), (g_2, m_2)), ((g_1, m_1), (g_2 + 1, m_2'))]$ or $[((g_1, m_1), (g_2, m_2)), ((g_1 + 1, m_1'), (g_2, m_2))]$. On each of these links, labeled by I, a qubit (spanned by $|\uparrow\rangle_I$ and $|\downarrow\rangle_I$) is placed, and the tensor product of all these two-dimensional vector spaces define the full Hilbert space of our system (which could be modified by Gauss's law, see below).

The Hamiltonian of the system is (see Fig. 3)

$$H = -J \sum_p B_p - h \sum_I X_I, \tag{1}$$

where X_I is the Pauli operator (other operator of interest is Z_I) on link I, p stands for a plaquette which consists of four links denoted by I/p $[((g_1, m_1), (g_2, m_2)), ((g_1 + 1, m_1'), (g_2, m_2))]$ (link along the "1-direction"), $[((g_1 + 1, m_1'), (g_2, m_2)), ((g_1 + 1, m_1'), (g_2 + 1, m_2'))]$ (link along the "2-direction"), $[((g_1, m_1), (g_2 + 1, m_2')), ((g_1 + 1, m_1'), (g_2 + 1, m_2'))]$, and $[((g_1, m_1), (g_2, m_2)), ((g_1, m_1), (g_2 + 1, m_2'))]$, such that

$$B_p = \prod_{I/p} Z_{I/p}. \tag{2}$$

Throughout the paper, we use the notation a/b to mean that all the a that touch b; here, for example, I/p means the set of all links I that bound the plaquette p.

The system is invariant to a local (gauge) transformation defined at any site s by

$$A_s = \prod_{I/s} X_{I/s}, \tag{3}$$

where I/s are the links that touch the site s. Of course, A_s commutes with B_p, for all s, p. The question we pose is the nature of the ground state as a function of h/J.

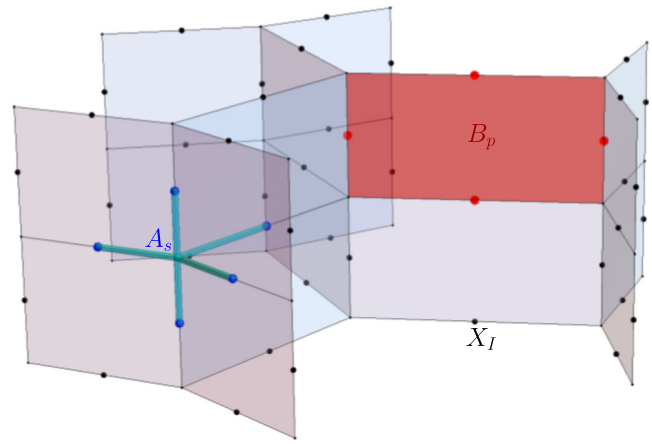

FIG. 3. Illustrating the definition of X_I, B_p, and A_s used the construction of the $\mathbb{Z}_2$ gauge theory. Qubits (small black circles) placed on the links (thin black lines) are labeled by I, and X_I is the Pauli X operator at link I. The term B_p is defined using the plaquette in light red where the product in Eq. (2) are over the four qubits (marked in red) that are on the links that define the plaquette. By the same token, the term A_s at site s of the arboreal lattice is defined using the product over the blue qubits [see Eq. (3)] connected to the site by the thick cyan lines.

B. Ground state and excitations

Taking $J > 0$, we see that a ground state of the system is $|\Uparrow\rangle = \prod_I |\uparrow\rangle_I$ such that $B_p = 1$ for all p. Excitations above the ground state are gapped; indeed, flipping the spin on the link along the 1-direction, e.g., $[((g_1, m_1), (g_2, m_2)), ((g_1 + 1, m_1'), (g_2, m_2))]$, flips k_2 plaquettes with an energy penalty of $2k_2J$. Similarly, flipping a spin on a link along the 2-direction produces k_1 plaquettes with $B_p = -1$ and an energy cost of $2k_1J$.

The ground state for small h, $h \ll J$ can be obtained by noting the gapped nature of the system at $h = 0$. We see, using standard perturbation theory, that the effective toric code Hamiltonian is

$$H_{\text{eff}} = -J \sum_p B_p - K \sum_s A_s, \tag{4}$$

where

$$K = C(k_1, k_2) \frac{h^{k_1+k_2}}{J^{k_1+k_2-1}} \tag{5}$$

and $C(k_1, k_2)$ is a positive number. We thus see that the ground state for $h \ll J$ requires $A_s = 1$, leading to

$$|\text{GS}, h \ll J\rangle = \prod_s (1 + A_s)|\Uparrow\rangle, \tag{6}$$

quite similar to what is found in the usual toric code [10]. Although the ground state bears a strong resemblance to that found in the usual toric code, there is more interesting physics in the arboreal arena.

Consider the excitations in the system. First, we have the electric charges of the gauge theory, described by states where $A_s = -1$. Just as in the toric code, a pair of these charges appear at the sites connected by the link I when we operate Z_I on the ground state, with an energy cost of 4 K. Remarkably, these two charges can be moved away" from each other arbitrarily far away" by successive operation of Z operators, while keeping the energy fixed. Just as the toric code, the arboreal $\mathbb{Z}_2$ gauge theory is thus electrically deconfined when $h \ll J$.

The crucial difference with the usual toric code is in the magnetic plaquette excitations or *monopoles*. Action of X_I on the link I on the ground state produces k_1 flipped plaquettes with an energy cost of $2k_1J$ if the link I is in the 2-direction, and k_2 flipped plaquettes with energy cost $2k_2J$ if the link I is in the 1-direction. The difference with the toric code is most easily seen when $k_2 \geqslant 2$. The set of $k_1(k_2)$ monopoles in the arboreal arena cannot be separated from each other while staying in the energy degenerate subspace, unlike in the usual two-dimensional toric code where the monopoles can be freely separated arbitrarily apart without recourse to any further excited states. One might suspect that the situation in the arboreal arena is akin to a toric code on a three-dimensional cubic lattice [66], but there is, again, a crucial difference. One can produce *an isolated monopole* (plaquette excitation) with energy $2J$ on the infinite arboreal arena, unlike in the three-dimensional toric code where plaquette excitations are necessarily associated with looplike entities. Stated in other words, the plaquette excitations are pointlike excitations in the two-dimensional arboreal arena (hence, naturally called monopoles), while the plaquette excitations of the three-dimensional toric code are looplike (not point) excitations. In particular, an *isolated monopole* with energy $2J$ can be created in an arboreal arena. This is readily demonstrated by an explicit construction. The state (see Fig. 4)

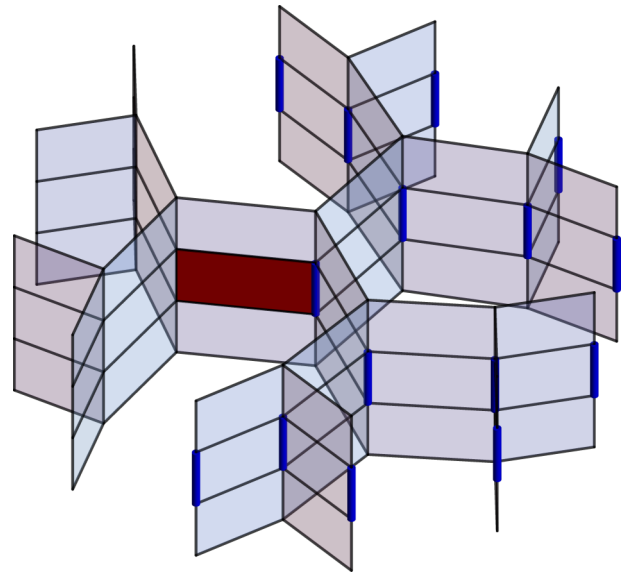

FIG. 4. An isolated monopole excitation with energy $2J$ created in an arboreal arena B(3)□B(2) created from the state $|\Uparrow\rangle$. The links with thick dark blue lines have flipped spins. The monopole in this case is a lineon. In the general B(k_1)□B(k_2) ($k_1, k_2 > 2$) arena for which an illustration is difficult, it is immobile, i.e., a fracton.

$$|M\rangle = X_{I(0,0)} \left(\prod_{g=1}^{\infty} \prod_{m_g=0}^{(k_1-1)^g} X_{I(g,m_g)} \right) |\text{GS}, h \ll J\rangle, \tag{7}$$

where

$$I(g, m_g) = \begin{cases} [((0,0),(0,0)),((0,0),(1,0))], & g = 0, m_g = 0 \\ [((g, m_g),(0,0)),((g, m_g),(1,0))], & g \neq 0 \end{cases} \tag{8}$$

contains an isolated monopole on the plaquette defined by the sites $((0,0),(0,0)),((0,0),(1,0)),((1,k_1-1),(1,0)),((1,k_1-1),(0,0))$. A key observation that follows is that if $k_2 > 2$, then the isolated monopole is *completely immobile*, since attempts to move it by local spin flips necessarily produces additional monopoles. However, when $k_2 = 2$, the monopole is mobile solely along the 2-direction as shown in Fig. 4. When $k_2 > 2$, the monopole is, thus, an immobile fracton, while for $k_2 = 2$ (extruded tree) the monopole is *lineon* as it can move freely along the 2-direction. We thus arrive at the inevitable conclusion that *even the simplest gauge theory on the arboreal arena is magnetically fractonic!*.

It is evident that arboreal areas can offer advantages of the toric code on a square lattice, where *both* electric and magnetic charges are fully mobile. We also note that we can achieve fractonicity of both electric and magnetic excitations

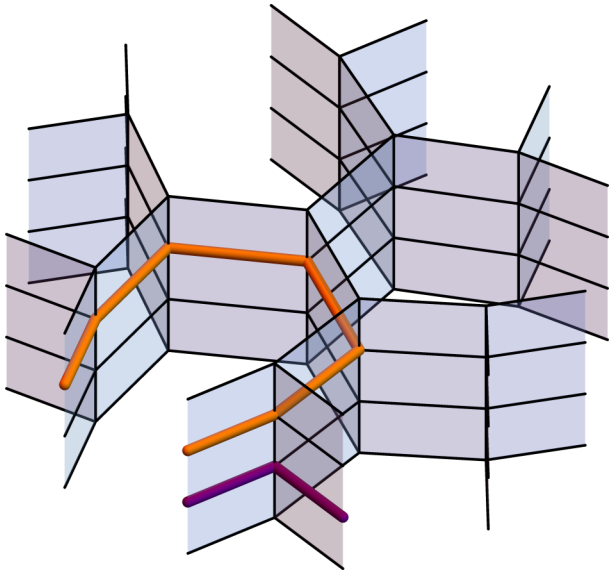

FIG. 5. Boundary operators and global Wilson lines in a finite arboreal arena. The purple solid line runs over the links such that the product of Z operators on these links defines a boundary operator. The orange solid line shows a global Wilson line (again a product of Z operators of all the links that make up the orange line).

if we construct the two-dimensional arboreal arena using hypertrees, and we leave this direction for future work.

C. Ground-state degeneracy

It is natural to enquire if the unique aspects of gauge theory on arboreal arenas uncovered above manifest in other properties such as the ground state degeneracy. This is best studied focusing on two-dimensional Cayley trees. The ground state degeneracy, and associated topological order, can be studied using finite systems with smooth and rough boundaries [67]. An important point to be noted in the construction of gauge theory on *finite* arboreal arenas is that, in addition to the B_p terms that are associated naturally to plaquettes that arise from the Cartesian product of graphs, there are additional gauge-invariant local operators that arise at the boundary. By local operators, we here mean the interactions that are defined on adjacent links (which share a site) such that the number of links are not more than four (the number of links that defines a plaquette). An instance of the boundary operator is illustrated in Fig. 5. One can have gauge-invariant boundary operators that are products of smaller boundary operators that are also gauge invariant. We keep only those operators which cannot be written as a product of other smaller gauge invariant operators. All such independent boundary operators that arise in the case of the rough boundaries are collectively denoted by H_∂,

$$H = -J\sum_p B_p - h\sum_I X_I + H_\partial, \tag{9}$$

commuting with the Hamiltonian.

We will obtain the ground state degeneracies D_G of two-dimensional Cayley trees by considering four cases. First, we consider completely smooth two-dimensional trees of the type $\mathrm{SC}(k_1)_{M_1}\square\mathrm{SC}(2)_{M_2}$, which is a smooth extruded Cayley tree. Here the number of qubits are

$$N_Q(\mathrm{SC}(k_1)_{M_1}\square\mathrm{SC}(2)_{M_2}) = \frac{k_1((k_1-1)^{M_1}+M_2(4(k_1-1)^{M_1}-2)-1)-4M_2}{k_1-2}. \tag{10}$$

The number of conserved plaquette operators B_p is

$$N_B(\mathrm{SC}(k_1)_{M_1}\square\mathrm{SC}(2)_{M_2}) = \frac{2k_1M_2((k_1-1)^{M_1}-1)}{k_1-2} \tag{11}$$

and the number of conserved charges are

$$N_A(\mathrm{SC}(k_1)_{M_1}\square\mathrm{SC}(2)_{M_2}) = \frac{(2M_2+1)(k_1(k_1-1)^{M_1}-2)}{k_1-2}. \tag{12}$$

There are no constraints on the B_p, but $\prod_s A_s = 1$ when the boundaries are smooth. Further, there are no boundary operators, i.e., $H_\partial = 0$. In this smooth two-dimensional Cayley tree, therefore, we see that the ground state is nondegenerate.

Next, we consider two-dimensional Cayley trees with rough boundaries. The first case we consider is $\mathrm{RC}(k_1)_{M_1}\square\mathrm{SC}(2)_{M_2}$, a rough extruded tree. The number of qubits in this case is

$$N_Q(\mathrm{RC}(k_1)_{M_1}\square\mathrm{SC}(2)_{M_2}) = \frac{k_1^2(2M_2+1)(k_1-1)^{M_1}-k_1((k_1-1)^{M_1}+2M_2+1)-4M_2}{k_1-2} \tag{13}$$

and the number of conserved plaquettes B_p is

$$N_Q(\mathrm{RC}(k_1)_{M_1}\square\mathrm{SC}(2)_{M_2}) = \frac{2k_1M_2((k_1-1)^{M_1+1}-1)}{k_1-2}, \tag{14}$$

while the number of conserved charges is the same as in Eq. (12). The new features here, as mentioned above, are the boundary terms H_∂; we keep a number of additional boundary-independent terms in the Hamiltonian that are gauge invariant and describe the interactions of four (or less) adjacent links. The number of such terms in H_∂ is

$$N_\partial(\mathrm{RC}(k_1)_{M_1}\square\mathrm{SC}(2)_{M_2}) = (k_1-2)k_1^2(k_1-1)^{M_1-2}, \tag{15}$$

each of which commutes with the Hamiltonian Eq. (9). There are no global constraints on the plaquettes, charges, or the boundary operators. We thus obtain the ground state degeneracy D_G,

$$\begin{aligned}\ln{}_2 D_G &= N_Q - (N_B + N_\partial + N_A)\\ &= k_1(k_1-1)^{M_1-2} - 1,\end{aligned} \tag{16}$$

which results in a degeneracy of the ground state whose logarithm scales as the exponential of the system size M_1! What is the origin of such large degeneracies? These degeneracies can be traced to the global Wilson line operators,

$$W(I_a, I_b) = \prod_{I=I_b}^{I_a} Z_I, \tag{17}$$

where the index I runs over links that provide the shortest path from boundary link I_b to I_a (see Fig. 5). It must be noted that these Wilson lines are not all of the same length. The shortest of them will be six links long, while the longest of them will contain links of the order M_1. Due to this reason, the degeneracy of the ground state is not topologically protected—perturbations that span over six links can mix states with distinct values of the short Wilson lines. However, if the perturbations are short ranged, spanning at most over $L \ll M_1$ links, a large number of these degenerate states cannot be perturbed, and degeneracy survives. This is akin to the topological protection of the ground state degeneracy in the toric code giving rise to the notion of topological order [5]. Taking a cue from this, we term the degeneracy induced by the large number of global Wilson lines to be *arboreal topological order*. This notion, along with a fractonic monopole excitation and a fully mobile charge excitation, provide a unique form of quantum matter in the arboreal arena.

Most interestingly, the large degeneracy discussed above is absent if the two-dimensional Cayley tree of the type $\mathrm{SC}(k_1)_{M_1}\square\mathrm{RC}(2)_{M_2}$ is considered (it be can shown that the degeneracy in this case is 2). This observation further corroborates in the importance of the tree structure ($k_1 > 2$) in providing for the large number of global Wilson lines.

We now consider the last type of extruded tree $\mathrm{RC}(k_1)_{M_1}\square\mathrm{RC}(2)_{M_2}$, where all boundaries are rough. Here the number of qubits are

$$N_Q(\mathrm{RC}(k_1)_{M_1}\square\mathrm{RC}(2)_{M_2}) = \frac{k_1((k_1(2M_2+1)+1)(k_1-1)^{M_1} - 2M_2 - 1) - 4(M_2+1)}{k_1-2}. \tag{18}$$

The number of conserved plaquettes is

$$N_B(\mathrm{RC}(k_1)_{M_1}\square\mathrm{RC}(2)_{M_2}) = \frac{2k_1(M_2+1)((k_1-1)^{M_1+1}-1)}{k_1-2}, \tag{19}$$

along with number charges being given [Eq. (12)]. There are no independent boundary terms when both Cayley trees are rough. Notably, there are constraints on B_p. Indeed, we have

$$\prod_{p\in\mathrm{WS}} B_p = 1, \tag{20}$$

where WP is a Wilson surface whose 1-direction is the global Wilson line and the 2-direction is along the 1D chain forming the $\mathrm{RC}(2)_{M_2}$ Cayley tree. The total number of such constraints are

$$N_C(\mathrm{RC}(k_1)_{M_1}\square\mathrm{RC}(2)_{M_2}) = k_1(k_1-1)^{M_1} - 1. \tag{21}$$

All these considerations result in the ground state degeneracy given by

$$\ln {}_2D_G = N_Q - (N_B + N_A - N_C) = 0. \tag{22}$$

The ground state of this system on the arboreal arena is nondegenerate, a feature that it shares with a fully rough square lattice toric code [67] defined by $\mathrm{RC}(2)_{M_1}\square\mathrm{RC}(2)_{M_2}$, which is also nondegenerate.

We can extend these considerations to generic two-dimensional Cayley lattices, i.e., with $k_1, k_2 > 2$. For $\mathrm{SC}(k_1)_{M_1}\square\mathrm{SC}(k_2)_{M_2}$, we find that the ground state is nondegenerate. For $\mathrm{RC}(k_1)_{M_1}\square\mathrm{SC}(k_2)_{M_2}$, the ground state degeneracy $\ln {}_2D_G(\mathrm{RC}(k_1)_{M_1}\square\mathrm{SC}(k_2)_{M_2}) \sim (k_1-1)^{M_1-2}$, with an analogous result for the smooth-rough case. For the rough-rough case, we, again, obtain a nondegenerate ground state.

D. Properties of excitations

As noted above, the excitations above the gapped ground state in the deconfined phase ($h \ll J$) of the gauge theory are the deconfined electric charges and the fractonic magnetic monopoles. We now discuss the generalized braiding properties of these excitations. Consider an isolated monopole [as discussed near equation Eq. (7)]. Consider any surface S (made up of plaquettes) containing this monopole plaquette such that a site at the boundary of this surface has an electric charge. We consider this surface to be simply connected in that it has no holes, etc. This charge can be transported around the monopole plaquette by the operator

$$T_e = \prod_{I\in\partial S} Z_I \tag{23}$$

such that the set of links on the boundary of S from a closed loop. The presence of the monopole is detected by the condition that $T_e = -1$, i.e., a deconfined electric charge will pick up an Aharonov-Bohm phase of π when transported around a magnetic monopole. This is most easily seen by using Fig. 6, where T_e, the product over the links on the boundary ∂S (cyan line in Fig. 6), is equal to the product of all B_p of the plaquettes p (shaded plaquettes enclosed by the cyan line in Fig. 6), which is clearly -1 as the plaquette shaded in red with the monopole alone contributes a -1.

Curiously, the process of transporting a monopole around an electric charge is not so straightforward on an arboreal arena. If, for example, the process used for the electric charge is applied with the role of the electric and magnetic charges reversed and a transport operator of the form $T_m = \prod_{I\perp\partial S} X_I$ (where I are now links not in included in the surface S, but attached to the boundary vertices), $T_m|\Psi\rangle$ will not, in general, restore the state back to $|\Psi\rangle$ which describes the state with the electric charge. To alleviate this problem, we consider a generalized braiding process by the following construction.

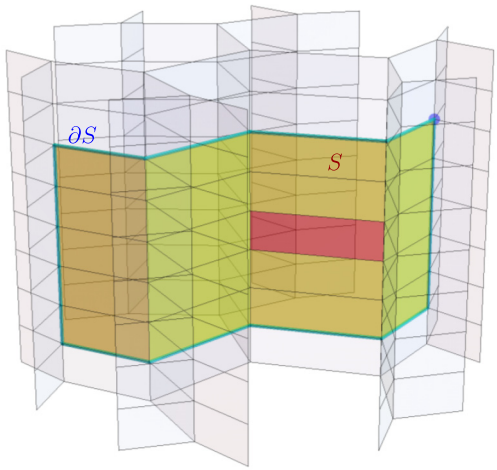

FIG. 6. Mutual statistics of an electric charge and magnetic monopole. S is a surface made of plaquettes (shown with a yellow hue) containing the monopole shown in red. The boundary ∂S of S is shown by cyan links. The blue point is the location of the electric charge, which is transported around the boundary ∂S by the operator defined in Eq. (23).

Consider an electric charge located at a site s_e (i.e., $A_{s_e} = -1$). Now consider a volume V that consists of this site. The volume V consists of a set of sites and links [i.e., is a subgraph of arboreal arena $\mathrm{B}(k_1)\square\mathrm{B}(k_2)$] such that every two sites are path connected, i.e., the volume is simply connected. Further, for any link present in V, both sites connected to it are present in V. A site in volume V is called an interior point if all the links incident on the site are present in the subgraph V. Thus, the boundary of V consists of vertices v in V such that some of the links of these vertices are not included in V. The links of the boundary points not included in V are the boundary links and denoted by $\mathcal{L}(\partial V)$. The volume V also does not contain any holes. This is ensured by the condition that there is a boundary path in connecting any two boundary points which contain only sites that are boundary sites. Now consider the operator

$$T_m = \prod_{I \in \mathcal{L}(\partial V)} X_I, \tag{24}$$

which acts on the boundary links of V (see Fig. 7). Although this operator does not enjoy the direct interpretation of the transport operators of monopole charges, it detects the presence of electric charges in volume V. Indeed, for the state $|\Psi\rangle$ with the electric charge at s_e discussed above, $T_m|\Psi\rangle = -|\Psi\rangle$. Further, this operator generalizes to any number of charges, as is immediately evident from the fact that $T_m = \prod_{s\in V} A_s$. As a concrete example of this, consider $\mathbb{Z}_2$ gauge theory defined on $\mathrm{B}(k_1)\square\mathrm{B}(k_2)$ with an electric charge present at the sites ((0,0),(0,0)). Now consider the subgraph $V = \mathrm{SC}(k_1)_{G_1}\square\mathrm{SC}(k_2)_{G_2}$, which is made of Cayley trees with G_1 and G_2 generations. The boundary links of V will now be those links that are present in $\mathrm{RC}(k_1)_{G_1}\square\mathrm{RC}(k_2)_{G_2}$ but not present in V. Indeed, it is immediate that $T_m = -1$, i.e., this operator detects the presence of the electric charge at ((0,0),(0,0)). This is evident from the fact that T_m is equal to the product of all A_s, where s are the sites in volume V, and only $A_{s_e} = -1$.

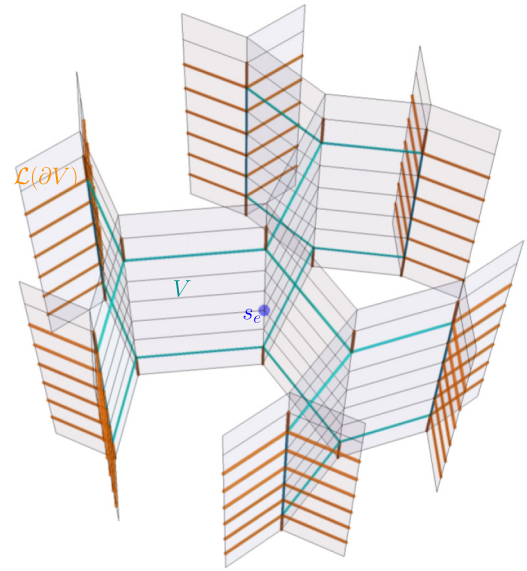

FIG. 7. Detecting the presence of an electric charge. The electric charge is located at the site s_e, i.e., $A_{s_e} = -1$ as indicated by the blue dot. This site is enclosed by a volume V inside the cyan lines, i.e., all sites and links enclosed by the cyan lines. The boundary links of this volume $\mathcal{L}(\partial V)$ are shown in orange and are used in Eq. (24).

E. Ground-state phases

Having established the state in the regime $h \ll J$, we investigate the opposite regime where $h \gg J$. For $J = 0$, the state is given by a product state $|\Rightarrow\rangle = \prod_I |\rightarrow\rangle_I$, where $X_I|\rightarrow\rangle_I = |\rightarrow\rangle_I$. The state is nondegenerate and gapped with a gap of order h. For finite J (with $h/J \gg 1$), we see that plaquette terms only produce a change of the ground state energy of order $J^2/(8h)$ and the state $|\Rightarrow\rangle$ continues to be the ground state. Further, the electric charges are confined—two adjacent charges can be separated over L links only via an energy penalty of order $2Lh$.

These observations raise the natural question apropos the nature of quantum transition from the deconfined arboreal ordered state to a confined state up on the tuning of h. We explore this question using a variational approach aimed at understanding the overall physics [68–70]. We work in the sector of the Hilbert space that imposes the Gauss's law, $A_s = 1$. The (unnormalized) wave function we use is

$$|\mathrm{GS}(b)\rangle = \left[\prod_p (1 + bB_p)\right] |\Rightarrow\rangle, \tag{25}$$

where b is a real variational parameter and $|\Rightarrow\rangle = \prod_I \frac{1}{\sqrt{2}}(|\uparrow\rangle_I + |\downarrow\rangle_I)$. The ground state occurs when $b = b_{\mathrm{GS}}$ at which $\langle \mathrm{GS}(b)|H|\mathrm{GS}(b)\rangle / \langle \mathrm{GS}(b)|\mathrm{GS}(b)\rangle$ is minimized. This variational state recovers the exact ground state for $h \ll J$ when $b_{\mathrm{GS}} = 1$, and the ground state $|\Rightarrow\rangle$ for $h \gg J$ when $b_{\mathrm{GS}} = 0$. Any nonanalytic behavior of $b_{\mathrm{GS}} = 0$ as a function of h/J is an indicator of a phase transition.

The details of the variational calculations are presented in Supplemental Material S1 [71]. Here we describe the key results. First, we note that the variational state Eq. (25) recovers the continuous phase transition of the $\mathbb{Z}_2$-gauge theory

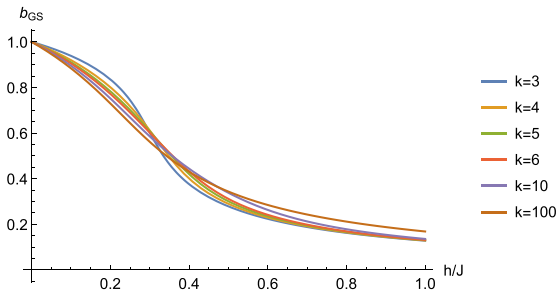

FIG. 8. Plot of b_{GS} as a function of h/J for a $\mathbb{Z}_2$ gauge theory Eq. (9) defined on $SC(k)_M\square SC(2)_{M_2}$–extruded k-Cayley trees with smooth-smooth boundaries with M, M_2 large. There is no quantum phase transition and topological order does not persist at finite h for any $k \geqslant 3$.

on the square lattice at $h_c = 0.25J$ (to be compared with the exact result of $0.22J$ (cf. Ref. [72]), albeit with Landau critical exponents.

The physics in the arboreal arena is richer. Starting with extruded trees, we see that boundary conditions of the tree play a crucial role in determining the phases of the gauge theory on the arboreal arena. For $SC(k)_M\square SC(2)_{M_2}$, we find that in the limit of large M, M_2, the state changes smoothly up on the tuning of h/J (see Fig. 8). On the other hand, for $RC(k)_{M_1}\square SC(2)_{M_2}$, the system does encounter a phase transition (Fig. 9). Quite interestingly, the nature phase transition found in this variational description depends on the value of k. For $k = 3$ and $k = 4$, the transition is *first order*, while for $k \geqslant 5$, the transition is continuous. For $k = 3$, the critical value $h_c \approx 0.418625J$ and for $k = 4$, $h_c \approx 0.49295J$. For $k \geqslant 5$, the continuous quantum phase transition occurs at $h_c = J/2$ as can be obtained from analytical considerations. The same results are obtained for fully rough extruded k-Cayley trees $[RC(k)_M\square RC(2)_{M_2}]$.

Considering more general two-dimensional arboreal lattices with $k_1, k_2 > 2$, we find that both $SC(k_1)_{M_1}\square SC(k_2)_{M_2}$ and $RC(k_1)_{M_1}\square SC(k_2)_{M_2}$ do not undergo a phase transition with increasing h, i.e., there is no deconfined phase in these

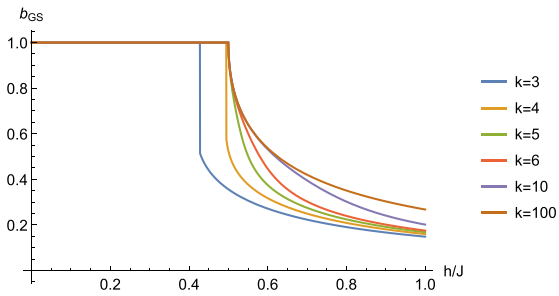

FIG. 9. Plot of b_{GS} as a function of h/J for a $\mathbb{Z}_2$ gauge theory Eq. (9) defined on $RC(k)_M\square SC(2)_{M_2}$–extruded k-Cayley trees with rough-smooth boundaries (M, M_2 large). There is a deconfined phase for $h < h_c$ and a confined phase for $h > h_c$. The transition is first order for $k = 3$ ($h_c \approx 0.42J$) and $k = 4$ ($h_c = 0.49J$). For all $k \geqslant 5$, a continuous transition from the deconfined to the confined phase occurs at $h_c = J/2$. The same results are obtained for fully rough trees of the type $RC(k)_M\square RC(2)_{M_2}$.

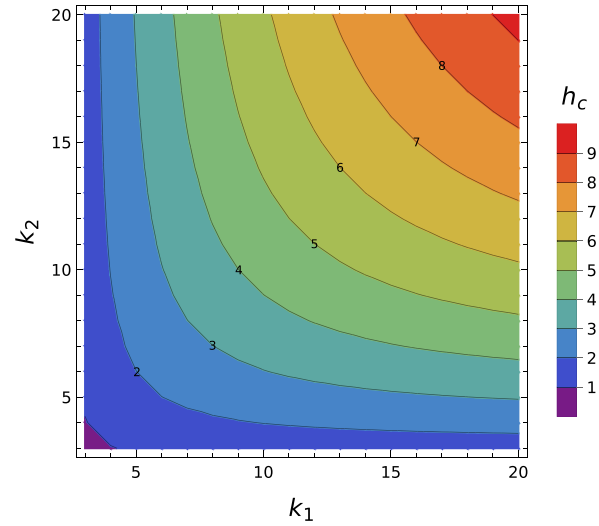

FIG. 10. Critical value h_c of h for general finite arboreal lattices $RC(k_1)_{M_1}\square RC(k_2)_{M_2}$ ($k_1, k_2 > 2$, M_1, M_2 large) with rough boundaries. There is a deconfined phase for $h < h_c$ and a confined phase for $h > h_c$.

systems. The rough-rough Cayley trees $RC(k_1)_{M_1}\square RC(k_2)_{M_2}$, on the other hand, have a first-order transition up on increase of h. In these systems, there is a deconfined phase for $h < h_c$ and a confined phase for $h > h_c$. The dependence of h_c on k_1 and k_2 is plotted in Fig. 10. For $k_1 = k_2$, h_c increases monotonically and approximately linearly with increasing k_1 ($h_c \approx 0.5k_1$ for large k_1). On the other hand, keeping k_1 fixed, and increasing k_2, h_c saturates to a value determined by the fixed value of k_1.

F. Dual models

The results discussed above raise a set intriguing questions pertaining to the crucial role played by the boundary conditions on the phases obtained in the arboreal arena. While this may not be unexpected considering the fact that the number of boundary degrees of freedom of the arboreal arena are of the same order as the number of bulk degrees of freedom, significant insights are obtained by constructing and studying dual models.

1. Arboreal Kramers-Wannier duality

Before we discuss models dual to gauge theories defined in general arboreal arenas, we note that many of the dualities that we uncover can be elucidated using a basic duality in a hyper-Bethe lattice which we dub the arboreal Kramers-Wannier duality. Consider a GQIM defined on a Hilbert space of qubits placed on the sites of a hypertree $HB(k, n)$ with the Hamiltonian

$$H = -J\sum_I \left(\prod_{s/I} Z_s\right) - h\sum_s X_s. \tag{26}$$

Here I labels the links and s the sites, respectively, of $HB(k, n)$. The first term defines the generalized Ising interaction on the hyperlink I that is a product of Z operators on n sites that belong to hyperlink I. Interestingly, this GQIM

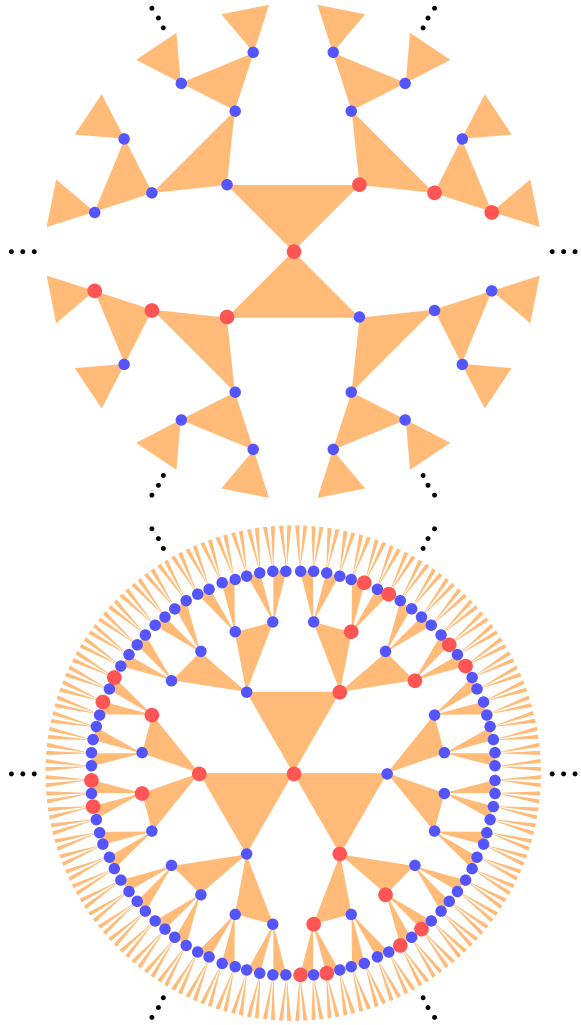

FIG. 11. The subsystem symmetry operators for the GQIM are given by applying X on the highlighted (red) spins as shown. Note that the symmetry operators for GQIM on HB(2, 3) and HB(3, 3) live on B(2) and B(3), respectively.

has a *subsystem symmetry* for all $n > 2$, in that flipping spins on a subset of sites S (such as those shown in Fig. 11), described by the transformation operator $U_S = \prod_{s\in S} X_s$, leaves the Hamiltonian H [Eq. (26)] invariant. There are many such distinct subsets of sites, and these generate all the subsystem symmetries.

To find a dual, we introduce a second set of qubits located at the *centers* of the links I, and define operators $\tilde{Z}_I$ and $\tilde{X}_I$ that act on them (see Fig. 12). We then make the following identifications:

$$\tilde{X}_I \equiv \prod_{s/I} Z_s, \tag{27}$$

$$\prod_{I/s} \tilde{Z}_I \equiv X_s, \tag{28}$$

that preserve all the necessary algebraic relations between the operators X_s and $\prod_{s/I} Z_s$. The dual Hamiltonian is

$$\tilde{H} = -J \sum_I \tilde{X}_I - h \sum_s \left(\prod_{I/s} \tilde{Z}_I \right), \tag{29}$$

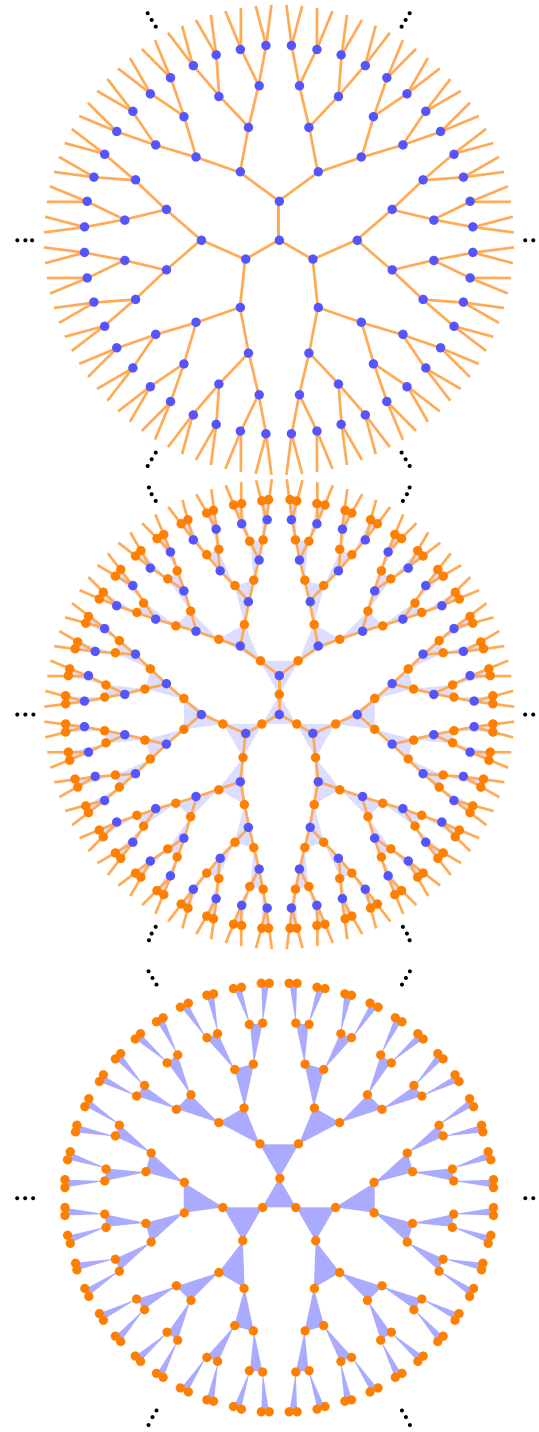

FIG. 12. Illustrating the generalized Kramers-Wannier duality of generalized quantum Ising models on HB(k, n) and HB(n, k). Color scheme shows the mapping between sites and edges. Dual qubits (orange dots) are placed at the centers of the links of the top panel as shown in the middle panel. Hyperlinks (light blue triangles) are defined using the dual qubits to obtain the dual hypertree shown in the bottom panel.

where I defines *sites* and s defines the links of a hyper-Bethe lattice HB(n, k) (see Fig. 12). This dual model also has a subsystem symmetry analogous to the original model provided $k > 2$. Since the lattice is infinite, we have, from Eq. (27), that $\prod_{I\in S'} \tilde{X}_I = 1$, where S' is the subset of sites

as shown in Fig. 11, and similarly $\prod_{s\in S} X_s = 1$ (following Eq. (28), see Ref. [73]). We thus conclude that the GQIM defined on HB(k, n) is dual to GQIM defined on HB(n, k), when restricted to the subsystem symmetry singlet sectors of both models. This is the statement of the arboreal Kramers-Wannier duality.

2. *Dual of $\mathbb{Z}_2$ gauge theory*

Armed with the arboreal Kramers-Wannier duality, we next construct a model dual to the $\mathbb{Z}_2$ gauge theory [Eq. (1)] defined on B$(k)\square$B(2), i.e., an infinite extruded tree. Recall that the Hilbert space of this theory is defined by a set of qubits (Q) that reside on the links of this extruded tree, and satisfy the Gauss's law constraint $A_s = 1$, for all sites s. The key sets of operators that act on this Hilbert space are B_p, plaquette operators where p labels the plaquettes, and X_I the transverse field operators on the links labeled by I. These operators satisfy the following relations:

$$\begin{aligned}
&[B_p, B_{p'}] = 0, \forall \text{ plaquettes } p, p',\\
&[X_I, X_{I'}] = 0, \forall \text{ links } I, I',\\
&[B_p, X_I] = 0, \text{ if link } I \text{ is not a part of the plaquette } p,\\
&\{B_p, X_I\} = 0, \text{ if link } I \text{ is part of the plaquette } p,
\end{aligned} \tag{30}$$

with [,] and {, } denoting, respectively, the commutator and anticommutator. Note that there are two types of links, labeled by I_1, which are along the 1-direction, or tree direction, and by I_2 which are along the 2-direction, or extrusion direction. To obtain the dual model, we define a different Hilbert space made of qubits ($\tilde{Q}$) placed at the centers of each plaquette and define operators $\tilde{Z}_p$ and $\tilde{X}_p$ that act on these new qubits, which are naturally labeled by the plaquette p. We make the following dual identifications:

$$\begin{aligned}
B_p &\equiv \tilde{X}_p,\\
X_{I_1} &\equiv \prod_{p/I_1} \tilde{Z}_p,\\
X_{I_2} &\equiv \prod_{p/I_2} \tilde{Z}_p,
\end{aligned} \tag{31}$$

where the links I_1 and I_2 are, as described above, along the 1 and 2 directions, respectively. Note that the product p/I_2 runs over k plaquettes and thus X_{I_2} dualizes to a k-qubit generalized Ising interaction. Similarly, X_{I_1} dualizes to a 2-site Ising interaction. The resulting dual Hamiltonian is

$$\tilde{H} = -J \sum_p \tilde{X}_p - h \sum_{I_1} \left(\prod_{p/I_1} \tilde{Z}_p \right) - h \sum_{I_2} \left(\prod_{p/I_2} \tilde{Z}_p \right). \tag{32}$$

A study of Fig. 13 reveals that this is a GQIM defined on a two-dimensional hypertree HB$(2, k)\square$HB$(2, 2)$. Most interestingly, this dual model has a subsystem Ising symmetry, where transformation $U_W = \prod_{p\in W} \tilde{X}_p$ leaves the system unchanged. Here, the plaquettes p belong to W, the global Wilson surface of the $\mathbb{Z}_2$ gauge theory on the extruded tree introduced earlier (see Figs. 5 and 13). Every distinct global Wilson surface W produces a symmetry operation U_W that acts only on a subset of qubits and in this sense is a subsystem.

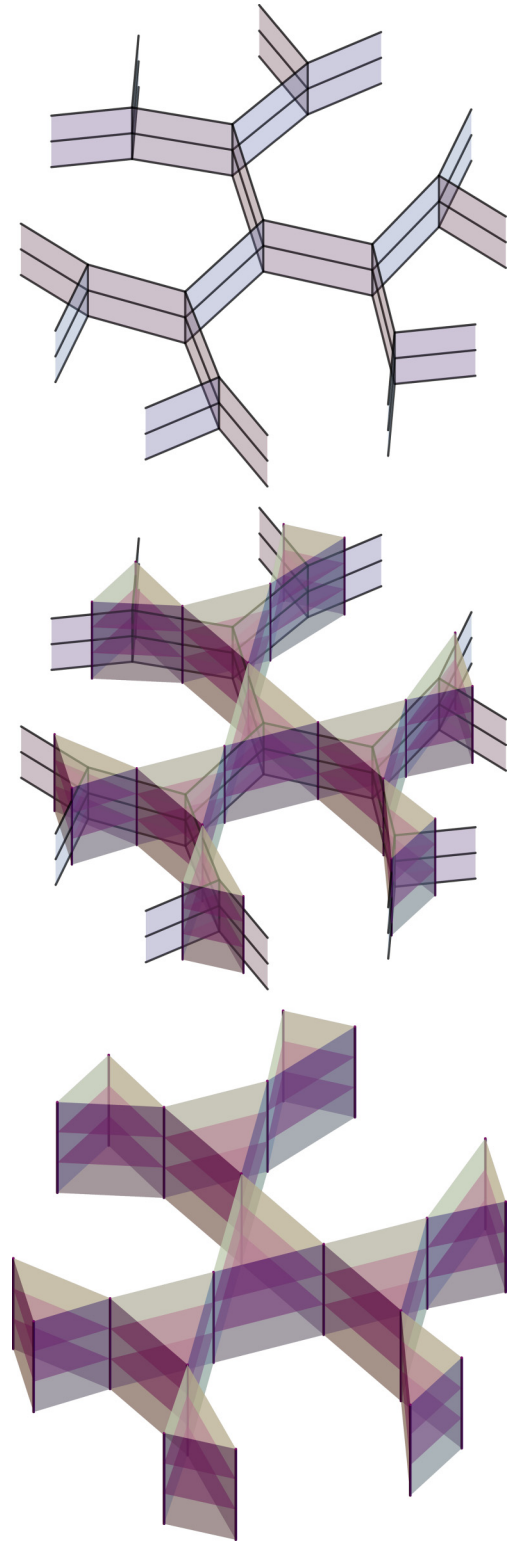

FIG. 13. Theory dual to $\mathbb{Z}_2$ gauge theory defined on B(3)$\square$B(2) (extruded tree). Construction of the dual is analogous to Fig. 12. Dual qubits are placed at the centers of the plaquettes of the top panel and connected by hyperlinks as shown in the middle panel. The resulting dual model defined on HB(2, 3)$\square$HB(2, 2) is shown in the bottom panel.

Of course, viewed from the perspective of the original operators $U_W = \prod_{p\in W} B_p$ which are constrained, i.e., $\prod_{p\in W} B_p = 1$ since each qubit in a plaquette is shared by one other plaquette in W. This forces $U_W = 1$. Further, the dual identification also imposes constraints on 't-Hooft operators of the gauge theory. For example, consider the operator $U_T = \prod I \in TX_I$, where I are links in $T = \{[((g, m_g), (0, 0)), ((g, m_g), (1, 0))]\}$, were (g, m_g) is a tree coordinate on $\mathrm{B}(k)$. By the duality construction, $U_T = \prod_I \prod_{p/I} \tilde{Z}_p = 1$, i.e., we obtain a 't-Hooft operator constraint $U_T = 1$. All such independent constraints have to be satisfied on the gauge theory side of the duality.

The consideration above allows us to arrive at a remarkable conclusion: the theory dual to $\mathbb{Z}_2$ gauge theory H [Eq. (1)] with Gauss's law constraint ($A_s = 1, \forall s$) and constraints on the independent 't-Hooft operators, defined on $\mathrm{B}(k)\square\mathrm{B}(2)$, is the GQIM [Eq. (32)] defined on $\mathrm{HB}(2, k)\square\mathrm{HB}(2, 2)$ in its singlet sector of its subsystem symmetry. This result also provides a nice connection to earlier work. Many known fractonic gauge theories defined on lattices (such as the X-cube model) are dual to models with subsystem symmetries. Indeed, as we discussed above, the simple $\mathbb{Z}_2$ gauge theory [Eq. (1)] defined on $\mathrm{B}(k)\square\mathrm{B}(2)$ does support fractonic excitations, and its duality to the GQIMon $\mathrm{HB}(2, k)\square\mathrm{HB}(2, 2)$ with subsystem symmetries fits nicely into this picture.

Finally, we mention the model dual to a $\mathbb{Z}_2$ gauge theory defined on a general two-dimensional arboreal lattice $\mathrm{B}(k_1)\square\mathrm{B}(k_2)$ with an imposed Gauss's law constraint $A_s = 1$. Using the procedure developed above, we see that the dual theory is the GQIM defined on two-dimensional arboreal lattice $\mathrm{HB}(2, k_1)\square\mathrm{HB}(2, k_2)$. This GQIM has a set of subsystem symmetries constructed using the Wilson surfaces of the gauge theory, and duality holds in the singlet sector of all generators of the subsystem symmetries. The duality also operates in the sectors of the gauge theory where all the independent 't-Hooft operators are constrained to identity as discussed above. These results can be generalized to higher dimensional arboreal lattices.

3. *Duals to $\mathbb{Z}_2$ gauge theory on finite arboreal lattices*

We will now explore the dualities in finite arboreal lattices. First, consider a GQIM defined on a smooth hyper-Cayley tree $\mathrm{SHC}(k, n)_M$. This tree consists of sites s that are bulk sites and boundary sites (sites of the Mth generation), while all links I are bulk links. The Hamiltonian is the same as Eq. (26) and this system possesses subsystem symmetries effected by simultaneous spin flips on the subset of sites S such as shown in Fig. 11.

On the rough hyper-Cayley tree $\mathrm{RHC}(k, n)_M$, all the sites s are bulk sites while there are both bulk links and boundary links (which are the last set of links). The GQIM is defined as

$$H = -J \sum_{I\in\text{bulk links}} \left(\prod_{s/I} Z_s\right) - J \times \sum_{I_\partial\in\text{boundary links}} Z_{s/I_\partial} - h\sum_s X_s. \tag{33}$$

Note that this Hamiltonian does not have any global flip symmetries and the definition is motivated by the anticipation of a duality.

We can naturally extend the definition of GQIM to higher dimensional arboreal lattices with boundaries. Indeed, a GQIM defined on $\mathrm{SHC}(k_1, n_1)_{M_1}\square\mathrm{SHC}(k_2, n_2)_{M_2}$ has a Hamiltonian

$$H = -J \sum_{I_1} \underbrace{\left(\prod_{s/I_1} Z_s\right)}_{n_1\text{terms}} - J \sum_{I_2} \underbrace{\left(\prod_{s/I_2} Z_s\right)}_{n_2\text{terms}} - h\sum_s X_s, \tag{34}$$

where $I_{1,2}$ are hyperlinks along the 1 and 2 directions, respectively. This model, again, has a large number of subsystem symmetries whenever $k_1, k_2 > 2$. More general higher dimensional lattices with different boundary conditions can similarly be defined.

We now show that GQIM defined on $\mathrm{SHC}(k, n)_M$ is dual to a GQIM defined on $\widetilde{\mathrm{RHC}}(n, k)_M$ (see Table I for definitions). To this end, identify each link I of $\mathrm{SHC}(k, n)_M$ with a *site* of $\widetilde{\mathrm{RHC}}(n, k)_M$ on which a dual qubit is placed. For each link I of $\mathrm{SHC}(k, n)_M$, define

$$\tilde{X}_I \equiv \prod_{s/I} Z_s. \tag{35}$$

Further, associate with each bulk site s of $\mathrm{SHC}(k, n)_M$ a hyperlink of $\widetilde{\mathrm{RHC}}(n, k)_M$ (this dual hyperlink will touch all the dual sites that are the hyperlinks $\mathrm{SHC}(k, n)_M$ which touch the site s), and define

$$\prod_{I/s} \tilde{Z}_I \equiv X_s, \quad s \in \text{bulk sites of } \mathrm{SHC}(k, n)_M. \tag{36}$$

We now see that the boundary sites of $\mathrm{SHC}\ (k, n)_M$ will be identified with the dual *boundary links* of $\widetilde{\mathrm{RHC}}(n, k)_M$, such that

$$\tilde{Z}_{I/s_\partial} \equiv X_{s_\partial}, \quad s_\partial \in \text{boundary sites of } \mathrm{SHC}(k, n)_M. \tag{37}$$

We see the Hamiltonian Eq. (26) defined on $\mathrm{SHC}(k, n)_M$ dualizes to

$$\tilde{H} = -J \sum_I \tilde{X}_I - h \sum_{s\in\text{bulk sites}} \times \left(\prod_{I/s} \tilde{Z}_I\right) - h \sum_{s_\partial\in\text{boundary sites}} \tilde{Z}_{I/s_\partial}, \tag{38}$$

which is exactly the GQIM defined on $\widetilde{\mathrm{RHC}}(n, k)_M$ with coupling constants J and h interchanged [see Eq. (33)]. Finally, consider $\prod_{s\in S} X_s$ which defines a subsystem symmetry transformation of the GQIM defined on $\mathrm{SHC}(k, n)_M$ on the subsystem S, see Fig. 11. This operator, under duality, maps to

$$\prod_{s\in S}\prod_I \tilde{Z}_{I/s} = 1, \tag{39}$$

where the right-hand side becomes identity owing to the fact that every $\tilde{Z}$ operator appears twice in the expression. In other words, the duality operates in the singlet sector of all the subsystem symmetries of GQIM defined on $\mathrm{SHC}(k, n)_M$.

TABLE II. Summary of dualities. Most of the dualities operate in the singlet sectors of certain operators on either side of the duality. GQIM: Generalized quantum Ising model [Eq. (26) and Eq. (33)], $\mathbb{Z}_2$-GT: $\mathbb{Z}_2$ gauge theory [Eq. (1) and Eq. (9)], X-cube-GT: X-cube gauge theory [Eq. (48)]. GFIM: Generalized quantum face Ising model—this is the generalization of GQIM to include only face interactions. The arenas are as described in Table I. The first three dualities are for infinite arboreal arenas, while the remainder are on finite systems.

Model		Dual model	
Hamiltonian	Arena	Hamiltonian	Arena
GQIM	$\mathrm{HB}(k,n)$	GQIM	$\mathrm{HB}(n,k)$
$\mathbb{Z}_2$-GT	$\mathrm{B}(k_1)\square\mathrm{B}(k_2)$	GQIM	$\mathrm{HB}(2,k_1)\square\mathrm{HB}(2,k_2)$
X-cube-GT	$\mathrm{B}(k_1)\square\mathrm{B}(k_2)\square\mathrm{B}(k_3)$	GFIM	$\mathrm{HB}(2,k_1)\square\mathrm{HB}(2,k_2)\square\mathrm{HB}(2,k_3)$
GQIM	$\mathrm{SHC}(k,n)_M$	GQIM	$\widetilde{\mathrm{RHC}}(n,k)_M$
GQIM	$\mathrm{RHC}(k,n)_M$	GQIM	$\widetilde{\mathrm{SHC}}(n,k)_{M+1}$
$\mathbb{Z}_2$-GT	$\mathrm{SHC}(k_1,n_1)_{M_1}\square\mathrm{SHC}(k_2,n_2)_{M_2}$	GQIM	$\widetilde{\mathrm{RHC}}(n_1,k_1)_{M_1}\square\widetilde{\mathrm{RHC}}(n_2,k_2)_{M_2}$
$\mathbb{Z}_2$-GT	$\mathrm{RHC}(k_1,n_1)_{M_1}\square\mathrm{RHC}(k_2,n_2)_{M_2}$	GQIM	$\widetilde{\mathrm{SHC}}(n_1,k_1)_{M_1+1}\square\widetilde{\mathrm{SHC}}(n_2,k_2)_{M_2+1}$
$\mathbb{Z}_2$-GT	$\mathrm{SHC}(k_1,n_1)_{M_1}\square\mathrm{RHC}(k_2,n_2)_{M_2}$	GQIM	$\widetilde{\mathrm{RHC}}(n_1,k_1)_{M_1}\square\widetilde{\mathrm{SHC}}(n_2,k_2)_{M_2+1}$

The discussion above provides a platform for us to discuss the theory dual to $\mathbb{Z}_2$ gauge theory defined on $\mathrm{SC}(k_1)_{M_1}\square\mathrm{SC}(k_2)_{M_2}$. By placing dual qubits on the faces of the plaquettes of the arboreal lattice, and performing identifications similar to Eq. (31), we see that dual theory is a GQIM defined on $\widetilde{\mathrm{RHC}}(2,k_1)_{M_1}\square\widetilde{\mathrm{RHC}}(2,k_2)_{M_2}$. The rough boundaries arise from the identification of X operators at the boundary qubits of $\mathrm{SC}(k_1)_{M_1}\square\mathrm{SC}(k_2)_{M_2}$ with the $\tilde{Z}$ operators on the sites of $\widetilde{\mathrm{RHC}}(2,k_1)_{M_1}\square\widetilde{\mathrm{RHC}}(2,k_2)_{M_2}$ that host its boundary links. The Gauss's law constraint of the gauge theory is identically satisfied in its dual description. Importantly, the duality imposes a constraint on the some operators of the gauge theory. Indeed, a class of 't-Hooft operators $\prod_{I\in T}X_I=\prod_{I\in T}(\prod_{p/I}\tilde{Z}_I)=1$. Thus, all such 't-Hooft operators are constrained to be identity on the gauge theory side of the duality, a condition analogous to that discussed in the case without boundaries.

Turning now to the $\mathbb{Z}_2$ gauge theory defined on $\mathrm{RC}(k_1)_{M_1}\square\mathrm{RC}(k_2)_{M_2}$, we see immediately that theory is dual to GQIM defined on $\widetilde{\mathrm{SHC}}(2,k_1)_{M_1+1}\square\widetilde{\mathrm{SHC}}(2,k_2)_{M_2+1}$ with the dual qubits, placed again on the faces of the plaquettes of $\mathrm{RC}(k_1)_{M_1}\square\mathrm{RC}(k_2)_{M_2}$, and the dualization effected via Eq. (31). Now, there are restrictions on the subsystem symmetries of the dual GQIM defined on $\widetilde{\mathrm{SHC}}(2,k_1)_{M_1+1}\square\widetilde{\mathrm{SHC}}(2,k_2)_{M_2+1}$ arising from the constraints imposed by 'surfaces' such as the Wilson surfaces discussed above for $\prod_{p\in W}\tilde{X}_p=\prod_{p\in W}B_p=1$. Thus the duality operates in the singlet sector of the subsystem symmetries of the dual GQIM defined on $\widetilde{\mathrm{SHC}}(2,k_1)_{M_1+1}\square\widetilde{\mathrm{SHC}}(2,k_2)_{M_2+1}$.

Finally, we note that the $\mathbb{Z}_2$ gauge theory defined on $\mathrm{SC}(k_1)_{M_1}\square\mathrm{RC}(k_2)_{M_2}$ is dual to GQIM defined on $\widetilde{\mathrm{RHC}}(2,k_1)_{M_1}\square\widetilde{\mathrm{SHC}}(2,k_2)_{M_2+1}$ using the procedure outlined above. The duality operates in the singlet sector 't-Hooft operators along the 1-direction. The dualities discussed here are summarized in Table II. The table also contains dualities of fractonic models which will be discussed in the next section.

4. Insights from dualties

The dualities developed above allow us to obtain further insights into the phases of the gauge theory discussed earlier using the variational approach. We exploit the duality between $\mathbb{Z}_2$ gauge theory defined on $\mathrm{B}(k_1)\square\mathrm{B}(k_2)$ and GQIM defined on $\mathrm{HB}(2,k_1)\square\mathrm{HB}(2,k_2)$ by redefining the coupling constants of the $\mathbb{Z}_2$ gauge theory Eq. (1) via $J\to J/\lambda$ and $h\to\lambda J$, where J (on the right-hand side) is an energy scale. The dual GQIM on $\mathrm{HB}(2,k_1)\square\mathrm{HB}(2,k_2)$ is obtained as

$$\tilde{H}=-\frac{J}{\lambda}\sum_p\tilde{X}_p-\lambda J\sum_{I_1}\underbrace{\left(\prod_{p/I_1}\tilde{Z}_{p/I_1}\right)}_{k_2\ \tilde{Z}\text{ operators}}-\lambda J\sum_{I_2}\underbrace{\left(\prod_{p/I_2}\tilde{Z}_{p/I_2}\right)}_{k_1\ \tilde{Z}\text{ operators}},\tag{40}$$

where p are plaquettes and $I_{1,2}$ are the links in the 1,2-directions of $\mathrm{B}(k_1)\square\mathrm{B}(k_2)$; ps labels the sites, and I_1, I_2 label the hyperlinks of $\mathrm{HB}(2,k_1)\square\mathrm{HB}(2,k_2)$. The Trotterized finite temperature partition function of this model is

$$\beta\tilde{H}=-K_\tau\sum_{I_\tau}\left(\prod_{p/I_\tau}Z_{p/I_\tau}\right)-K\sum_{I_1}\left(\prod_{p/I_1}\tilde{Z}_{p/I_1}\right)-K\sum_{I_2}\left(\prod_{p/I_2}\tilde{Z}_{p/I_2}\right),\tag{41}$$

where p, I_1, I_2, I_τ are the sites and hyperlinks of the a *three*-dimensional arboreal arena $\mathrm{HB}(2,k_1)\square\mathrm{HB}(2,k_2)\square\mathrm{HB}(2,2)$. Here $K_\tau=-\frac{1}{2}\ln(\tanh(\Delta\tau J/\lambda))$ and $K=\Delta\tau\lambda J$. Taking $K_\tau=K$, we see that Eq. (41) is a generalized *classical* Ising model defined on $\mathrm{HB}(2,k_1)\square\mathrm{HB}(2,k_2)\square\mathrm{HB}(2,2)$. The key point here is that any thermal phase transition at finite K of this model describes the quantum phase transition of the $\mathbb{Z}_2$ gauge theory defined on $\mathrm{B}(k_1)\square\mathrm{B}(k_2)$.

We now study the phases of the theory Eq. (41) using the Bragg-Williams mean-field ansatz. Defining $m=\langle\tilde{Z}_p\rangle$ (where $\langle a\rangle$ stands for the thermal average of the quantity a), we get

the self-consistency relation,

$$m = \tanh\left(K \sum_{\alpha=1}^{D} 2m^{k_\alpha - 1}\right), \tag{42}$$

where $D = 3$, $\alpha = 1, 2, 3$ and 3 is the τ direction [74]. An analysis of Eq. (42) reveals that whenever $k_1, k_2 > 2$, we obtain a first-order transition, i.e., there is a K_c at which a finite m nontrivial solution appears. On the other hand, if $k_1 = 2$, we obtain a first-order transition for $k_2 = 3, 4$, while for $k_2 \geqslant 5$ a continuous transition is obtained where a nonzero solution of m begins to appear for $K \geqslant K_c$ with the solution vanishing at $K = K_c$. It is reassuring that the results obtained from this dual picture qualitatively match the results obtained using the variational approach apropos the nature of the transition from the confined to the deconfined phase.

Finally, the duality analysis also offers insight into why the $\mathbb{Z}_2$ gauge theory defined on arboreal lattices with smooth boundaries do not have a phase transition (see Fig. 8). As discussed, the dual to this theory is a GQIM defined on an arboreal lattice with *rough boundaries*. This entails extra boundary terms [see Eq. (33)] which act like a boundary magnetic field along the z direction on the boundary spins (dual qubits). It is natural that no phase transition occurs in the system due to large number boundary spins which experience this field.

IV. FRACTONIC MODELS ON ARBOREAL ARENAS

A. X-cube model

In this section, we explore fracton models defined on the arboreal arenas. We will focus particularly on the X-cube model [27] defined on a three-dimensional arboreal arena. Consider a three-dimensional arboreal lattice $\mathrm{B}^3(k_1, k_2, k_3) \equiv \mathrm{B}(k_1)\square\mathrm{B}(k_2)\square\mathrm{B}(k_3)$, where $k_1, k_2, k_3 > 2$ with sites denoted by s and links denoted by I. The links of this arboreal lattice can be naturally classified as 1-links, 2-links, and 3-links, indicating their direction (or the parent tree to which they belong). To aid the discussion, we introduce an index α which can take values 1,2,3. Further, $\alpha' = 2, 3, 1$ and $\alpha'' = 3, 1, 2$, respectively, for $\alpha = 1, 2, 3$.

A set of links of this arboreal arena can act as the bounding links of cubes with 12 edges. For example, using the coordinate system defined on $\mathrm{B}(k_1)$, $\mathrm{B}(k_2)$, $\mathrm{B}(k_3)$ (see Sec. II), the following 12 links (s_1, s_2), (s_2, s_3), (s_3, s_4), (s_4, s_1), (s_5, s_6), (s_6, s_7), (s_7, s_8), (s_8, s_5), (s_1, s_5), (s_2, s_6), (s_3, s_7), (s_4, s_8) make up a cube. Here the sites s_i are, for example,

$$\begin{aligned}
s_1 &= ((g_1, m_1), (g_2, m_2), (g_3, m_3)),\\
s_2 &= ((g_1 + 1, m_1'), (g_2, m_2), (g_3, m_3)),\\
s_3 &= ((g_1 + 1, m_1'), (g_2 + 1, m_2'), (g_3, m_3)),\\
s_4 &= ((g_1, m_1), (g_2 + 1, m_2'), (g_3, m_3)),\\
s_5 &= ((g_1, m_1), (g_2, m_2), (g_3 + 1, m_3')),\\
s_6 &= ((g_1 + 1, m_1'), (g_2, m_2), (g_3 + 1, m_3')),\\
s_7 &= ((g_1 + 1, m_1'), (g_2 + 1, m_2'), (g_3 + 1, m_3')),\\
s_8 &= ((g_1, m_1), (g_2 + 1, m_2'), (g_3 + 1, m_3')),
\end{aligned} \tag{43}$$

with m_α' are suitably chosen coordinates such that $((g_\alpha, m_\alpha), (g_\alpha + 1, m_\alpha'))$ is a link in $\mathrm{B}(k_\alpha)$. With these definitions, an α-link participates in $k_{\alpha'}k_{\alpha''}$ cubes. Similarly, a cube face with a normal in the α direction (this face has four links that define it, two in the α' direction and two in the α'' direction) is shared by k_α cubes. Finally, every site of the arena participates in $k_1k_2k_3$ distinct cubes.

To define the X-cube model on $\mathrm{B}^3(k_1, k_2, k_3)$, we introduce a qubit on every link of this three-dimensional arboreal arena. For every cube c, the magnetic term B_c is introduced as

$$B_c = \prod_{I/c} Z_{I/c}, \tag{44}$$

where I/c are 12 links that make up the cube c. Next, for each direction α, we can define the star operator defined at every site,

$$A_{s\alpha} = \prod_{I/s} X_I, \tag{45}$$

where I/s are $(k_{\alpha'} + k_{\alpha''})$ links that touch the site s in orthogonal directions to α. The X-cube model is defined as

$$H_{\text{X-cube}} = -J \sum_c B_c - K \sum_{s,\alpha} A_{s\alpha}, \tag{46}$$

where $J, K > 0$ are the energy scales.

It is easily verified that the operators B_c in Eq. (44) and $A_{s\alpha}$ in Eq. (45) commute with each other. A ground state of the model, which has $B_c = 1$ and $A_s = 1$ for all c and s, is

$$|\mathrm{GS}_{\text{X-cube}}\rangle = \prod_c (1 + B_c)|\Rightarrow\rangle, \tag{47}$$

where $|\Rightarrow\rangle = \prod_I (\frac{|\uparrow\rangle_I + |\downarrow\rangle_I}{2})$.

While the ground state of the X-cube model defined on the arboreal arena has very similar features as the X-cube model defined on the cubic lattice, the nature of excitations are different and interesting. Consider first the electric charge excitation at a site where two of the A operators have a value of -1. Such excitations can be created from the ground state by the application of the Z_I operator on a link I. If I is a 1-link, this will result in dipoles of $A_{s2} = -1$ and $A_{s3} = -1$ electric charge excitations (each of which cost an energy of 2 K) where $s = s_1, s_2$ are the two sites that define the chosen 1-link I. Pick another (any one of $k_1 - 1$ possibilities) 1-link I' emanating from the site s_2, and apply the operator $Z_{I'}$ to the state obtained after the application of Z_I. We see that the charges $A_{s_2(2,3)} = -1$ are transported to a new site s_3 as $A_{s_3(2,3)} = -1$, where s_3 is the other site of I', without any additional energy cost. More generally, for any given α, a charges $A_{s\alpha'} = -1$ and $A_{s\alpha''} = -1$ located at $s = ((g_1^o, m_1^o), (g_2^o, m_2^o), (g_3^o, m_3^o))$ can be transported to any point on the tree $\mathrm{B}(k_\alpha)$. For example, if $\alpha = 1$, then the charges can be transported to any other point $s' = ((g_1, m_1), (g_2^o, m_2^o), (g_3^o, m_3^o))$, where (g_1, m_1) is any other point on the tree $\mathrm{B}(k_1)$. We thus see that linenonic electric charges of the X-cube model defined on a cubic lattice, generalize to *treeonic* charges—charges with mobility restrictions constrained to a tree!

Consider now the monopole excitations where some cubes obtain $B_c = -1$. Such excitations are produced by application

of the X_I operator on the ground state at link I. When this link I is in the α direction, this process produces an excited state that is a bound state of $k_{\alpha'}k_{\alpha''}$ monopoles each with $B_c = -1$. For the X-cube model defined on a cubic lattice, this process will produce a bound state of four monopoles. However, in the cubic lattice, the quadrupole of monopoles can be split into two dipoles, and these dipoles can move freely in a plane. The situation is quite different in the arboreal arena. Consider $\alpha = 1$, i.e., link I is a 1-link. Application of X_I on the ground state will produce k_2k_3 monopoles. Now consider the application of a second X operator on a 1-link I' connected to a 2-link I_2 which, in turn, is connected to the original 1-link I. This whole process will produce a total of $2(k_2 - 1)k_3$ monopoles. In other words, the application of the second spin flip operator (in an attempt to move a subset of monopoles) will result in the creation of $(k_2 - 2)k_3$ *additional* monopoles. We thus see that in an arboreal three-dimensional lattice ($k_\alpha > 2$), there are no multipoles of B_c excitations that are mobile.

B. The gauge theory

We here study the X-cube gauge theory defined on a three-dimensional arboreal arena. We will consider an arena with boundaries focusing, among the variety of possibilities, on $\mathrm{RC}(k_1)_{M_1}\square\mathrm{RC}(k_2)_{M_2}\square\mathrm{RC}(k_3)_{M_3}$ with all rough boundaries, and $\mathrm{SC}(k_1)_{M_1}\square\mathrm{RC}(k_2)_{M_2}\square\mathrm{RC}(k_3)_{M_3}$ with one smooth boundary. The Hamiltonian we consider is

$$H_{\mathrm{XGT}} = -J\sum_c B_c - h\sum_I X_I + H_\partial, \tag{48}$$

where J and h are energy scales, B_c is the cube term [see Eq. (44)] defined on all allowed cubes, and X_I is the operator that acts of the qubit placed at link I. The Hamiltonian is invariant under local transformations generated by all the allowed operators $A_{s\alpha}$ defined at each site s [see Eq. (45)]. As in the case of the $\mathbb{Z}_2$-gauge theory, additional boundary terms arise, as these are invariant under the action of the local transformations generated by $A_{s\alpha}$ (see Supplemental Material [71]). The theory is studied in the gauge-invariant sector of the Hilbert space which satisfies the generalized Gauss's law:

$$A_{s\alpha} = 1. \tag{49}$$

When $h \ll J$, the theory Eq. (48) reduces to the X-cube model Eq. (46) in an infinite three-dimensional arboreal lattice. The ground state, in this regime, is in the deconfined phase of the theory. For large h, the ground state is the state $|\Rightarrow\rangle$ defined near Eq. (47), and is in the confined phase of the theory. In a three-dimensional cubic lattice, it is known that, upon increase of h from $h \ll J$ to $h \gg J$, a transition from the deconfined to confined phase occurs at a critical value of h via a first-order transition [70]. The natural question to address is the nature of the transition on the arboreal arena, and Eq. (48) is introduced on a finite system to aid this analysis.

Before we discuss the phase transition anticipated above, we will briefly describe the ground state degeneracy D_G of the system in the limit $h \ll J$. An explicit calculation shows

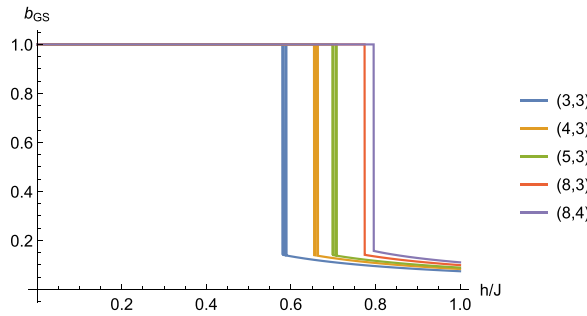

FIG. 14. Dependence of b_{GS} on h/J for the X-cube gauge theory defined on $\mathrm{SC}(k_1)_{M_1}\square\mathrm{RC}(k_2)_{M_2}\square\mathrm{RC}(2)_{M_3}$ for various (k_1, k_2) indicated in the legend. For large M_1, M_2, M_3, the transition from the confined to deconfined phase is first order.

that

$$\ln_2 D_G = (k_1((k_1-1)^{M_1-6} - 1)) \times \left(\left[\sum_{\gamma=2,3}\left(1 + \frac{k_\gamma((k_\gamma-1)^{M_\gamma}-1}{k_\gamma - 2}\right)\right] - 1\right) \tag{50}$$

for the case of X-cube gauge theory (with $h \ll J$, which is effectively the X-cube-model) defined on $\mathrm{RC}(k_1)_{M_1}\square\mathrm{SC}(k_2)_{M_2}\square\mathrm{SC}(k_3)_{M_3}$, taking into account the boundary operators allowed. Such a large degeneracy arises owing to the large number of Wilson line operators that become possible in the three-dimensional arboreal arena in a fashion similar to that illustrated in Fig. 5 for the $\mathbb{Z}_2$ gauge theory.

To study the evolution of the ground state as a function of h/J, we use the (unnormalized) variational ansatz similar to Eq. (25) as

$$|\mathrm{GS}(b)\rangle = \prod_c (1 + bB_c)|\Rightarrow\rangle, \tag{51}$$

where c also runs over all boundary terms in addition to the usual cube terms. The variational ground state is obtained for that value of b called b_{GS} at which the energy is minimized. The calculations are detailed in Supplemental Material S2 [71].

We first consider X-cube gauge theory defined on $\mathrm{SC}(k_1)_{M_1}\square\mathrm{RC}(k_2)_{M_2}\square\mathrm{RC}(2)_{M_3}$ where smooth boundaries are combined with rough boundaries. In these finite arboreal lattices, the third direction has $k_3 = 2$, i.e., this as an extruded three-dimensional arena. The main result, as seen from Fig. 14 is that the transition from the deconfined to confined phase occurs via a first-order transition for values of $k_1, k_2 \lesssim 10$ (see below). We also note that the transition is first order, in general, if all the boundaries are rough (results not shown).

Turning now to more general finite three-dimensional arboreal lattices with a smooth boundary $\mathrm{SC}(k_1)_{M_1}\square\mathrm{RC}(k_2)_{M_2}\square\mathrm{RC}(k_3)_{M_3}$, we find that the transition is generically first order as illustrated in Fig. 15. Similar results are shown for rough boundaries in Fig. 16. In fact, for some values of k, we find, as shown in Supplemental Material S2 [71], that there are *two* transitions, the first continuous

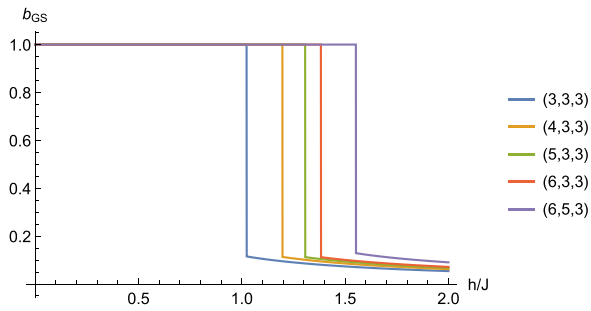

FIG. 15. Dependence of b_{GS} on h/J for the X-cube gauge theory defined on $SC(k_1)_{M_1}\square RC(k_2)_{M_2}\square RC(k_3)_{M_3}$, for various (k_1, k_2, k_3) indicated in the legend. For large M_1, M_2, M_3, a first-order transition from the deconfined to confined phase is obtained when the values of k_1, k_2, k_3 are small ($\lesssim 10$). For larger values of ks, a second-order transition from the confined to deconfined phase is obtained (see Supplemental Material S2 [71]).

one going from the deconfined to the confined phase, and a second first-order transition in the confined phase, indicating that there are two types of confined phases. Moreover, for very large values of ks, we find that the first-order transition between the confined phases is no longer present. The nature and physical underpinnings of these findings require further investigation which is a future direction to be pursued.

Finally, we note that the dual model (see Table II) to the X-cube gauge theory can be constructed (we do not elaborate this here) as generalized quantum face Ising models—face represents the fact that interaction terms are determined not by hyperlinks but by higher dimensional object such as faces and volumes formed by the hyperlinks). Such generalized quantum face Ising models will posses subdimensional symmetries, with the duality operating in the singlet sector of these symmetries along with the Gauss's law constraint on the gauge theory side and the 't-Hooft operator constraints. These results are natural generalizations of the dualities presented in Ref. [27] to arboreal arenas.

V. ARBOREAL TOPOLOGICAL AND FRACTON ORDERS

The results of the previous sections raise many interesting questions. For example, it is natural to inquire about the rela-

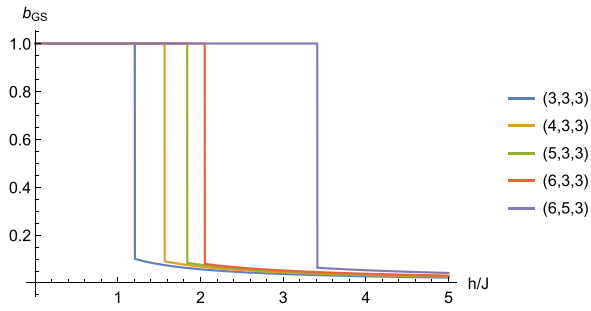

FIG. 16. Dependence of b_{GS} on h/J for the X-cube gauge theory defined on $RC(k_1)_{M_1}\square RC(k_2)_{M_2}\square RC(k_3)_{M_3}$, for various (k_1, k_2, k_3) indicated in the legend. A first-order transition from the deconfined to confined case is obtained for large M_1, M_2, M_3.

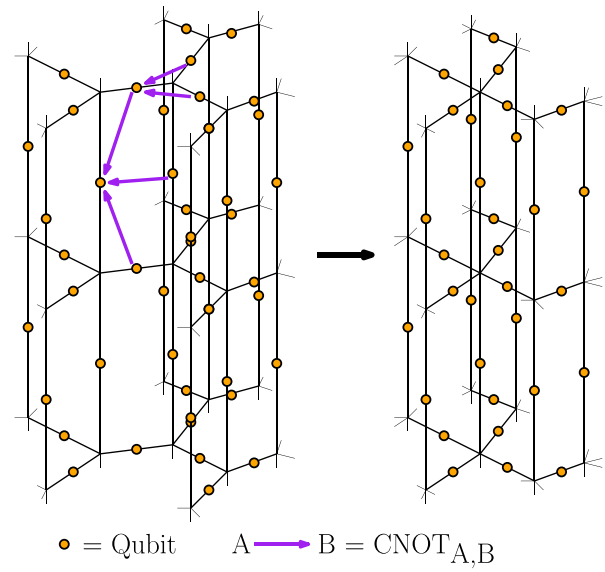

FIG. 17. Entanglement renormalization procedure demonstrating that the arboreal topological order on a B(3)□B(2) arena is equivalent to the one on B(4)□B(2). The CNOT operations indicated have to be performed between all pairs equivalent qubits, a process that is equivalent to a finite depth quantum circuit. The ground state of B(3)□B(2) is converted to that B(4)□B(2) produced with a set of qubits (not shown) in fixed states.

tionship between the arboreal topological order found in the $\mathbb{Z}_2$ gauge theory on B(k)□B(2) for different values of k. For example, are they different phases? How are they related? A key idea to be exploited in addressing these questions is that two systems are considered to be equivalent (same phase) if, for example, the ground state of one can be transformed to that of the other by a finite depth unitary quantum circuit [75,76] and a set of unentangled degrees of freedom. A generalization of this idea to fracton phases is also available, and will be discussed below.

To address these questions, consider the toric code Eq. (4) defined on B(3)□B(2). We use the entanglement renormalization process [75–77] to convert the ground state Eq. (6) of the toric code on B(3)□B(2) to that of the toric code on B(4)□B(2) times a set of unentangled qubits in fixed states. The procedure, demonstrated in Fig. 17, uses a set of CNOT gates (for details, see Ref. [75]) to produce a finite depth quantum circuit that acts on the toric code ground state on B(3)□B(2) to that of B(4)□B(2) produced with unentangled qubit states. It is immediately evident that this process converts the toric code ground state on B(k)□B(2) to that of B($k+1$)□B(2) whenever $k > 2$, suggesting that the arboreal topological order on B(k)□B(2) are equivalent for all $k > 2$. Note, however, that this order is distinct from the topological order on B(2)□B(2), the square lattice, as there is no finite depth unitary that will transform the toric code ground state on B(2)□B(2) to that of B(3)□B(2)!

These observations become more interesting when we note that the same process can be used to show that the arboreal topological order encoded in the ground state of the toric code defined on B(k_1)□B(k_2) when $k_1, k_2 > 2$ can be transformed to that of B(k_1+1)□B(k_2) (times unentangled qubits) or it

can be transformed to that of $\mathrm{B}(k_1)\square\mathrm{B}(k_2+1)$. This result is demonstrated as follows. Let $\mathcal{T}_x \equiv \{\mathcal{S}_x, \mathcal{L}_x\} = \mathcal{B}(3)$ and $\mathcal{T}_y \equiv \{\mathcal{S}_y, \mathcal{L}_y\} = \mathcal{B}(3)$. Consider a toric code model Eq. (4) defined by placing qubits on the links of $\mathcal{T} \equiv \{\mathcal{S}, \mathcal{L}\} = \mathcal{T}_x\square\mathcal{T}_y$. The set of sites can be written as

$$\mathcal{S} = \{(i, j') : i \in \mathcal{S}_x, j' \in \mathcal{S}_y\}. \tag{52}$$

Consider a single site $i \in \mathcal{S}_x$ and an associated link $\{i, j\} \in \mathcal{L}_x$. We will describe an entanglement renormalization transformation that fuses this link in $\mathcal{T}_x$ to a single point, therefore increasing its coordination by one. The entanglement renormalization transformation is done in two steps.

(1) For all $\{i', j'\} \in \mathcal{L}_y$, apply the following commuting gates:

(a) $\mathrm{CNOT}_{\{(i,i'),(j,i')\},\{(i,i'),(i,j')\}}$.

(b) $\mathrm{CNOT}_{\{(j,i'),(j,j')\},\{(i,i'),(i,j')\}}$.

(c) $\mathrm{CNOT}_{\{(i,j'),(j,j')\},\{(i,i'),(i,j')\}}$.

(2) For all links $\{i, k\} \in \mathcal{L}_x$ such that $k \neq j$, and all sites $i' \in \mathcal{S}_y$, apply $\mathrm{CNOT}_{\{(i,i'),(j,i')\},\{(i,i'),(k,i')\}}$.

Note that all CNOT gates in steps 1 and 2 commute and these CNOT gates act between nearby links, so this is a depth-1 process. CNOT gates act by conjugation as

$$\mathrm{CNOT}_{\alpha,\beta}: \begin{array}{ll} Z_\alpha I_\beta \to Z_\alpha I_\beta & Z_\alpha Z_\beta \leftrightarrow I_\alpha Z_\beta \\ X_\alpha I_\beta \leftrightarrow X_\alpha X_\beta & I_\alpha X_\beta \to I_\alpha X_\beta. \end{array} \tag{53}$$

After this transformation, we end up with product state qubits:

(a) For all $i' \in \mathcal{S}_y$, the qubit sitting on the link $\{(i, i'), (j, i')\}$ is in the state $|\rightarrow\rangle$.

(b) For all $\{i', j'\} \in \mathcal{L}_y$, the qubit sitting on the link $\{(i, i'), (i, j')\}$ is in the state $|\uparrow\rangle$.

Treating product states as a free resource, we remove them and end up with a toric code ground state on a new tree $\mathcal{T}_x'\square\mathcal{T}_y$, where $\mathcal{T}_x'$ is a modified B(3) with a single 4-coordinated site [see Fig. 18(a)].

We repeat this process $k-3$ (by now choosing a new link $\{i, j\}$ in $\mathcal{T}_x'$) times to create toric code ground states on $\mathcal{T}_x^{(k)}\square\mathcal{T}_y$, where $\mathcal{T}_x^{(k)}$ is a modified B(3) with a single k-coordinated site as shown in Fig. 18(b). Next, we repeat the above process for other sites and associated links in $\mathcal{T}_x^{(k)}$ to make all sites k coordinated, leaving us with $\mathcal{T}_x^{\mathrm{final}}$ a translation-invariant B(k). Repeating the same process for other sites can be done *in parallel*, i.e., this does not increase the circuit depth. Therefore, we have demonstrated that the toric code ground states on $\mathrm{B}(3)\square\mathrm{B}(3)$ and $\mathrm{B}(k)\square\mathrm{B}(3)$ are connected by a depth-$(k-3)$ circuit [see Fig. 18(c)].

We can repeat the same process for $\mathcal{T}_y$ using the same procedure. This leads us to conclude that the toric code ground state on $\mathrm{B}(3)\square\mathrm{B}(3)$ and $\mathrm{B}(k_x)\square\mathrm{B}(k_y)$ are connected by a depth-(k_x+k_y-6) circuit, for all $k_x, k_y \geqslant 3$. We thus arrive at a remarkable result that the arboreal topological orders encoded in the ground state of $\mathrm{B}(k_1)\square\mathrm{B}(k_2)$ for all $k_1, k_2 > 2$ are equivalent!

The above discussion allows us to classify arboreal orders of the toric code ground states. There are three types. First is the usual topological order of the toric code defined on the square lattice. The second is the arboreal topological order on extruded trees of the kind $\mathrm{B}(k)\square\mathrm{B}(2)$. The third one is the arboreal topological order on general two-dimensional arboreal lattices $\mathrm{B}(k_1)\square\mathrm{B}(k_2)$ with $k_1, k_2 > 2$. The common aspects of these three types of fracton orders may be understood from the perspective of their excitations. The toric code order realized in $\mathrm{B}(2)\square\mathrm{B}(2)$ (which is the the square lattice) has its magnetic monopole excitations fully mobile, this is the characteristic of the first type of topological order. On the other hand, the second type of order realized in $\mathrm{B}(k)\square\mathrm{B}(2)$ for $k > 2$ has mobility restrictions on the monopole, which can now move freely only along the vertical direction as shown in Fig. 4, i.e., the monopole excitations are lineons. The third kind of arboreal topological order realized in $\mathrm{B}(k_1)\square\mathrm{B}(k_2)$, $k_1, k_2 > 2$ has fully immobile monopole excitations.

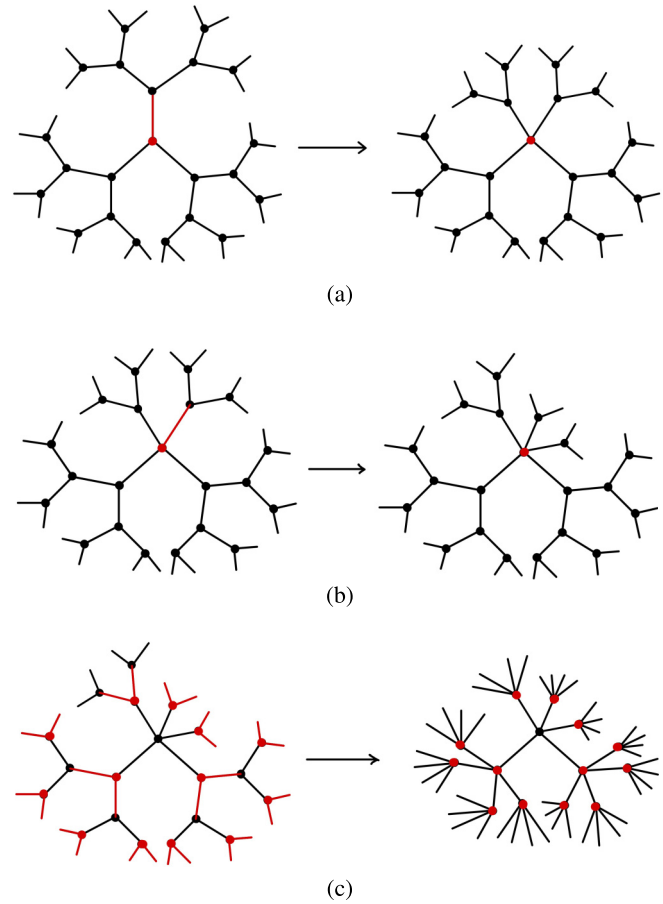

FIG. 18. Demonstrating the entanglement renormalization procedure that transforms the toric code on $\mathrm{B}(3)\square\mathrm{B}(3)$ to $\mathrm{B}(k)\square\mathrm{B}(k)$ ($k = 5$ is shown).

Moving to the fractonic models, we first observe that ideas from the notion of foliated fracton phases can be applied to understand and classify arboreal fracton orders. Using the notions introduced in Refs. [33,34], two fracton states are considered to be equivalent (in the same phase) if one can be transformed to another times unentangled layers of topologically ordered states and unentangled qubits in fixed states. By application of a finite depth quantum circuit process similar to the one shown in Fig. 17 (see Refs. [33,78]), the X-cube ground state Eq. (47) on $\mathrm{B}(k)\square\mathrm{B}(2)\square\mathrm{B}(2)$, $k > 2$ can be transformed to that of $\mathrm{B}(k+1)\square\mathrm{B}(2)\square\mathrm{B}(2)$ times unentangled toric code layers, each of which carries the topological order of the first kind discussed in the previous paragraph. This establishes the equivalence of the X-cube fracton order

on $B(k)\square B(2)\square B(2)$ for all $k > 2$. Similar arguments show that X-cube fracton order on $B(k_1)\square B(k_2)\square B(2)$ for $k_1, k_2 > 2$ are all equivalent. The key point to note here is that the finite depth quantum circuit transforms the X-cube ground state on $B(k_1)\square B(k_2)\square B(2)$ to that of $B(k_1+1)\square B(k_2)\square B(2)$ times uncoupled layers of topological order of the kind $B(k_2)\square B(2)$, i.e., the arboreal topological order of the second kind discussed in the paragraph above. Finally, X-cube orders on $B(k_1)\square B(k_2)\square B(k_3)$ with $k_1, k_2, k_3 > 2$ are all equivalent, in that the X-cube ground state on $B(k_1)\square B(k_2)\square B(k_3)$ can be transformed to that of $B(k_1+1)\square B(k_2)\square B(k_3)$ times unentangled layers, each of which carries an arboreal topological order of the third kind (see previous paragraph) on $B(k_2)\square B(k_3)$. This leads us to the conclusion that there are four types of X-cube fracton orders. The first one is the usual X-cube fracton order on a cubic lattice. The second is the X-cube order on $B(k)\square B(2)\square B(2)$ for all $k > 2$. The X-cube order on $B(k_1)\square B(k_2)\square B(2)$ for $k_1, k_2 > 2$ forms the third class. The fourth and final class is the X-cube fracton order on $B(k_1)\square B(k_2)\square B(k_3)$ for all $k_1, k_2, k_3 > 2$. Similar to that discussed for the arboreal topological order, the different fracton orders are also distinguished by the nature of the mobility of their excitations.

VI. CONCLUDING REMARKS

We conclude the paper with some remarks. First, we note that our work points to interesting possibilities that are offered by going beyond manifold arenas, as exemplified by the properties of the $\mathbb{Z}_2$-gauge theories of the arboreal arenas. Will such systems offer a fresh direction that enables them to be utilized gainfully for quantum information processing? Naturally, this entails costs in designing and constructing qubit connectivities and controls that are admittedly more complex. There have been encouraging recent advances where degrees of freedom are connected in unique geometries and topologies, see, for example, Refs. [79,80], which realize physics in hyperbolic geometry. These systems have exponential growth of sites with an increase in system size and require careful engineering of the components such as resonators that require a denser packing. Study of arboreal lattices will entail similar design concepts. The issue to be explored is that if such constructions provide cost-effective and efficient platforms for quantum information storage and processing. Further work is required to address this question. Second, we have explored only limited types of topological and fracton-ordered phases in the arboreal arena. It will be an interesting, if obvious, direction to explore the physics of models [15,81–83] that produce other types of orders. The physics of finite arboreal systems (with surfaces) also holds promise; for example, notions of gappability [84], etc. may be explored in this context.

ACKNOWLEDGMENTS

N.M. thanks the KVPY program and V.B.S. acknowledges DST, SERB for support. The authors thank Bhandaru Phani Parasar for critical comments on the paper.

[1] S. Ryu, A. P. Schnyder, A. Furusaki, and A. W. W. Ludwig, New J. Phys. **12**, 065010 (2010).
[2] A. Kitaev, AIP Conf. Proc. **1134**, 22 (2009).
[3] T. Senthil, Annu. Rev. Condens. Matter Phys. **6**, 299 (2015).
[4] C.-K. Chiu, J. C. Y. Teo, A. P. Schnyder, and S. Ryu, Rev. Mod. Phys. **88**, 035005 (2016).
[5] X.-G. Wen, Rev. Mod. Phys. **89**, 041004 (2017).
[6] M. Z. Hasan and C. L. Kane, Rev. Mod. Phys. **82**, 3045 (2010).
[7] X.-L. Qi and S.-C. Zhang, Rev. Mod. Phys. **83**, 1057 (2011).
[8] X. G. Wen, Int. J. Mod. Phys. B **04**, 239 (1990).
[9] C. Nayak, S. H. Simon, A. Stern, M. Freedman, and S. Das Sarma, Rev. Mod. Phys. **80**, 1083 (2008).
[10] A. Kitaev, Ann. Phys. **303**, 2 (2003).
[11] Y.-A. Chen, A. Kapustin, and D. Radicevic, Ann. Phys. **393**, 234 (2018).
[12] A. Kitaev and C. Laumann, arXiv:0904.2771
[13] B. M. Terhal, Rev. Mod. Phys. **87**, 307 (2015).
[14] B. J. Brown, D. Loss, J. K. Pachos, C. N. Self, and J. R. Wootton, Rev. Mod. Phys. **88**, 045005 (2016).
[15] M. A. Levin and X.-G. Wen, Phys. Rev. B **71**, 045110 (2005).
[16] C.-H. Lin, M. Levin, and F. J. Burnell, Phys. Rev. B **103**, 195155 (2021).
[17] E. Dennis, A. Kitaev, A. Landahl, and J. Preskill, J. Math. Phys. **43**, 4452 (2002).
[18] C. Castelnovo and C. Chamon, Phys. Rev. B **76**, 184442 (2007).
[19] Z. Nussinov and G. Ortiz, Phys. Rev. B **77**, 064302 (2008).
[20] C. Chamon, Phys. Rev. Lett. **94**, 040402 (2005).
[21] S. Bravyi, B. Leemhuis, and B. M. Terhal, Ann. Phys. **326**, 839 (2011).
[22] C. Castelnovo and C. Chamon, Philos. Mag. **92**, 304 (2012).
[23] J. Haah, Phys. Rev. A **83**, 042330 (2011).
[24] B. Yoshida, Phys. Rev. B **88**, 125122 (2013).
[25] S. Bravyi and J. Haah, Phys. Rev. Lett. **111**, 200501 (2013).
[26] S. Vijay, J. Haah, and L. Fu, Phys. Rev. B **92**, 235136 (2015).
[27] S. Vijay, J. Haah, and L. Fu, Phys. Rev. B **94**, 235157 (2016).
[28] D. J. Williamson, Phys. Rev. B **94**, 155128 (2016).
[29] T. H. Hsieh and G. B. Halász, Phys. Rev. B **96**, 165105 (2017).
[30] R. M. Nandkishore and M. Hermele, Annu. Rev. Condens. Matter Phys. **10**, 295 (2019).
[31] M. Pretko, X. Chen, and Y. You, Int. J. Mod. Phys. A **35**, 2030003 (2020).
[32] K. Slagle and Y. B. Kim, Phys. Rev. B **97**, 165106 (2018).
[33] W. Shirley, K. Slagle, Z. Wang, and X. Chen, Phys. Rev. X **8**, 031051 (2018).
[34] W. Shirley, K. Slagle, and X. Chen, SciPost Phys. **6**, 015 (2019).
[35] C. Xu, Phys. Rev. B **74**, 224433 (2006).
[36] A. Rasmussen, Y.-Z. You, and C. Xu, arXiv:1601.08235.
[37] M. Pretko, Phys. Rev. B **95**, 115139 (2017).
[38] M. Pretko, Phys. Rev. B **96**, 035119 (2017).
[39] S. Pai and M. Pretko, Phys. Rev. B **97**, 235102 (2018).
[40] V. B. Shenoy and R. Moessner, Phys. Rev. B **101**, 085106 (2020).
[41] M. Pretko, Phys. Rev. B **98**, 115134 (2018).
[42] N. Seiberg, SciPost Phys. **8**, 50 (2020).

[43] M. Pretko and L. Radzihovsky, Phys. Rev. Lett. **121**, 235301 (2018).
[44] A. Gromov, Phys. Rev. Lett. **122**, 076403 (2019).
[45] A. Gromov and P. Surówka, SciPost Phys. **8**, 65 (2020).
[46] N. Manoj, R. Moessner, and V. B. Shenoy, Phys. Rev. Lett. **127**, 067601 (2021).
[47] H. Kleinert, *Gauge Fields in Condensed Matter* (World Scientific, Singapore, 1989), Vol. 2.
[48] J. Dietel and H. Kleinert, Phys. Rev. B **73**, 024113 (2006).
[49] J. Zaanen, Z. Nussinov, and S. Mukhin, Ann. Phys. **310**, 181 (2004).
[50] A. J. Beekman, J. Nissinen, K. Wu, K. Liu, R.-J. Slager, Z. Nussinov, V. Cvetkovic, and J. Zaanen, Phys. Rep. **683**, 1 (2017).
[51] K. Slagle and Y. B. Kim, Phys. Rev. B **96**, 195139 (2017).
[52] Y. You, T. Devakul, S. L. Sondhi, and F. J. Burnell, Phys. Rev. Res. **2**, 023249 (2020).
[53] K. Slagle, Phys. Rev. Lett. **126**, 101603 (2021).
[54] N. Seiberg and S.-H. Shao, SciPost Phys. **10**, 3 (2021).
[55] J. I. Cirac and P. Zoller, Nat. Phys. **8**, 264 (2012).
[56] A. Blais, S. M. Girvin, and W. D. Oliver, Nat. Phys. **16**, 247 (2020).
[57] C. Song, D. Xu, P. Zhang, J. Wang, Q. Guo, W. Liu, K. Xu, H. Deng, K. Huang, D. Zheng, S.-B. Zheng, H. Wang, X. Zhu, C.-Y. Lu, and J.-W. Pan, Phys. Rev. Lett. **121**, 030502 (2018).
[58] K. J. Satzinger, Y.-J. Liu, A. Smith, C. Knapp, M. Newman, C. Jones, Z. Chen, C. Quintana, X. Mi, A. Dunsworth, C. Gidney, I. Aleiner, F. Arute, K. Arya, J. Atalaya, R. Babbush, J. C. Bardin, R. Barends, J. Basso, A. Bengtsson *et al.*, Science **374**, 1237 (2021).
[59] G. Semeghini, H. Levine, A. Keesling, S. Ebadi, T. T. Wang, D. Bluvstein, R. Verresen, H. Pichler, M. Kalinowski, R. Samajdar, A. Omran, S. Sachdev, A. Vishwanath, M. Greiner, V. Vuletić, and M. D. Lukin, Science **374**, 1242 (2021).
[60] V. Voloshin, *Introduction to Graph and Hypergraph Theory* (Nova Science Publishers, New York, 2009).
[61] C. J. Thompson, J. Stat. Phys. **27**, 441 (1982).
[62] R. Baxter, *Exactly Solved Models in Statistical Mechanics*, Dover Books on Physics (Dover Publications, New York, 2013).
[63] G. D. Mahan, Phys. Rev. B **63**, 155110 (2001).
[64] A. Georges, G. Kotliar, W. Krauth, and M. J. Rozenberg, Rev. Mod. Phys. **68**, 13 (1996).
[65] M. Nakahara, *Geometry, Topology and Physics*, 2nd ed. (Institute of Physics Publishing, Bristol, UK, 2003).
[66] C. Castelnovo and C. Chamon, Phys. Rev. B **78**, 155120 (2008).
[67] S. B. Bravyi and A. Y. Kitaev, arXiv:quant-ph/9811052.
[68] S. Dusuel and J. Vidal, Phys. Rev. B **92**, 125150 (2015).
[69] D. A. Reiss and K. P. Schmidt, SciPost Phys. **6**, 78 (2019).
[70] M. Mühlhauser, M. R. Walther, D. A. Reiss, and K. P. Schmidt, Phys. Rev. B **101**, 054426 (2020).
[71] See Supplemental Material at http://link.aps.org/supplemental/10.1103/PhysRevB.107.165136 for details of the variational calculations.
[72] I. S. Tupitsyn, A. Kitaev, N. V. Prokof'ev, and P. C. E. Stamp, Phys. Rev. B **82**, 085114 (2010).
[73] D. Radicevic, arXiv:1809.07757.
[74] A more general result for the self-consistency for a generalized classical Ising model on d dimensional arboreal arena $\square_{\alpha=1}^{D}\mathcal{H}B(k_\alpha, n_\alpha)$ reads $m = \tanh\left(K\sum_{\alpha=1}^{d} k_\alpha m^{n_\alpha - 1}\right)$.
[75] G. Vidal, Phys. Rev. Lett. **99**, 220405 (2007).
[76] X. Chen, Z.-C. Gu, and X.-G. Wen, Phys. Rev. B **82**, 155138 (2010).
[77] L. Tagliacozzo and G. Vidal, Phys. Rev. B **83**, 115127 (2011).
[78] A. Dua, P. Sarkar, D. J. Williamson, and M. Cheng, Phys. Rev. Res. **2**, 033021 (2020).
[79] A. J. Kollár, M. Fitzpatrick, and A. A. Houck, Nature (London) **571**, 45 (2019).
[80] A. Chen, H. Brand, T. Helbig, T. Hofmann, S. Imhof, A. Fritzsche, T. Kießling, A. Stegmaier, L. K. Upreti, T. Neupert, T. Bzdušek, M. Greiter, R. Thomale, and I. Boettcher, Nat. Commun. **14**, 622 (2023).
[81] K. Walker and Z. Wang, Front. Phys. **7**, 150 (2012).
[82] C. W. von Keyserlingk, F. J. Burnell, and S. H. Simon, Phys. Rev. B **87**, 045107 (2013).
[83] W. Shirley, K. Slagle, and X. Chen, Phys. Rev. B **102**, 115103 (2020).
[84] S. Ganeshan and M. Levin, Phys. Rev. B **105**, 155137 (2022).